Cosmogenic ages indicate no MIS 2 refugia in the Alexander Archipelago, Alaska

Caleb K. Walcott[1], Jason P. Briner[1], James F. Baichtal[2], Alia J. Lesnek[3], Joseph M. Licciardi[4]

[1]Department of Geology, University at Buffalo, Buffalo, NY 14260, USA

[2]Tongass National Forest, Thorne Bay, AK 99919, USA

[3]School of Earth and Environmental Sciences, CUNY Queens College, Flushing, NY 11367, USA

[4]Department of Earth Sciences, University of New Hampshire, Durham, NH 03824, USA

Correspondence to: Caleb K. Walcott (ckwalcot@buffalo.edu)

Abstract

The late-Pleistocene history of the coastal Cordilleran Ice Sheet remains relatively unstudied compared to chronologies of the Laurentide Ice Sheet. Yet accurate reconstructions of Cordilleran Ice Sheet extent and the timing of ice retreat along the Pacific Coast are essential for paleoclimate modeling, assessing meltwater contribution to the North Pacific, and determining the availability of ice-free land along the coastal Cordilleran Ice Sheet margin for human migration from Beringia into the rest of the Americas. To improve the chronology of Cordilleran Ice Sheet history in the Alexander Archipelago, Alaska, we applied ^{10}Be and ^{36}Cl dating to boulders and glacially sculpted bedrock in areas previously hypothesized to have remained ice-free throughout the local Last Glacial Maximum (LLGM; 20-17 ka). Results indicate that these sites, and more generally the coastal northern Alexander Archipelago, became ice-free by 15.1 ± 0.9 ka (n = 12 boulders; 1 SD). We also provide further age constraints on deglaciation along the southern Alexander Archipelago and combine our new ages with data from two previous studies. We determine that ice retreated from the outer coast of the southern Alexander Archipelago at

27   16.3 ± 0.8 ka (n = 14 boulders; 1 SD). These results collectively indicate that areas above

28   modern sea level that were previously mapped as glacial refugia were covered by ice during the

29   LLGM until between ~16.3 and 15.1 ka. As no evidence was found for ice-free land during the

30   LLGM, our results suggest that previous ice-sheet reconstructions underestimate the regional

31   maximum Cordilleran Ice Sheet extent, and that all ice likely terminated on the continental shelf.

32   Future work should investigate whether presently submerged areas of the continental shelf were

33   ice-free.

35   **1 Introduction**

36   The late-Pleistocene history of the coastal Cordilleran Ice Sheet remains relatively

37   unstudied compared to chronologies of the Laurentide Ice Sheet (; Dalton et al., 2020).

38   Cordilleran Ice Sheet margin reconstructions from the Pacific Coast are based largely on

39   qualitative field observations with little chronologic control (Dyke, 2004; Carrara et al., 2007;

40   Dalton et al., 2020). While a few studies have recently generated local ice sheet retreat

41   chronologies from terrestrial locations along the Pacific Coast (Darvill et al., 2018; Lesnek et al.,

42   2018; Lesnek et al., 2020),- there are still large areas of the southeastern Alaskan coastline that

43   lack direct age constraints on deglaciation (Fig. 1). Much of the Northern Hemisphere was

44   covered by continental ice sheets during the global Last Glacial Maximum (GLGM; ~26 – 19

45   ka). Chronologies of northern hemisphere glaciation have revealed that while the Laurentide Ice

46   Sheet and many alpine glaciers worldwide were at their greatest extents during the global Last

47   Glacial Maximum (GLGM; ~26-19 ka), the coastal Cordilleran Ice Sheet and the Puget Lobe

48   reached their maximum size ~20 – 17 cal ka (local Last Glacial Maximum; hereafter LLGM ;

49   Porter and Swanson, 1998; Booth et al., 2003; Praetorius and Mix, 2014; Darvill et al., 2018;

50   Lesnek et al., 2018). Other studies have also explored the Cordilleran Ice Sheet contributions to

51   meltwater pulse 1A (~14.6 ka) following the saddle collapse between the Laurentide Ice Sheet

52   and Cordilleran Ice Sheet (Gregoire et al., 2016; Ivanovic et al., 2017). Improved constraints on

53   Cordilleran Ice Sheet history around the time of meltwater pulse 1A are necessary to elucidate

54   any influences of coastal Cordilleran Ice Sheet configuration and retreat on saddle collapse.

55   Additionally, numerical modeling studies show differing responses of the Cordilleran Ice Sheet

56   to last deglacial climate oscillations, thus highlighting the need for an improved Cordilleran Ice

57   Sheet chronology to bolster model improvement and validation (Tarasov et al., 2012; Seguinot et

58   al., 2014; Gregoire et al., 2016; Seguinot et al., 2016; Ivanovic et al., 2017). Finally, a temporally

59   accurate paleogeographic reconstruction of the coastal Cordilleran Ice Sheet margin is required

60   to assess whether a viable coastal route existed for early Americans migrating from Beringia into

61   the Americas. This route hinges on the presence of ice-free land (refugia) suitable for human

62   habitation during the migration event(s). Earlier mapping efforts and other supporting

63   information indicate areas of potential refugia along the former coastal Cordilleran Ice Sheet

64   margin (Demboski et al., 1999; Cook et al., 2001; Carrara et al., 2003; Carrara et al., 2007;

65   Shafer et al., 2010; Shafer et al., 2011; Hebda et al., 2022).

66   This study has two goals: 1) improve the spatio-temporal patterns of coastal Cordilleran

67   Ice Sheet deglaciation in southeastern Alaska, and 2) assess whether areas of the northern

68   Alexander Archipelago mapped as refugia were ice-free throughout the LLGM and thus

69   available for human habitation (Fig. 2). We report 25 new cosmogenic ^{10}Be exposure ages from

70   boulders and bedrock in the northern Alexander Archipelago – the first exposure ages

71   documenting Cordilleran Ice Sheet retreat from this coastal region. We also report four ^{10}Be and

72   four cosmogenic ^{36}Cl ages from Suemez Island in the southern Alexander Archipelago. Our data

73 constrain the deglaciation of the marine-terminating Cordilleran Ice Sheet margin and expand the

74 overall North Pacific coastal glacial chronology. Our results suggest deglaciation of coastal

75 regions ~15.4 – 14.8 ka in the northern Alexander Archipelago and do not support previous

76 mapping of refugia in areas that are presently above sea level.

77

78 **2 Setting**
79
80   The Alexander Archipelago, southeast Alaska, stretches ~480 km (Fig. 2) along the

81 western coast of British Columbia. The southern part of the archipelago is dominated by Prince

82 of Wales Island and surrounding islands, whereas the northern part encompasses Baranof and

83 Chichagof Islands and a collection of smaller islands. The Alexander Archipelago consists of

84 accreted terranes (Triassic to Cretaceous in age) with quartz-bearing diorite and granodiorite

85 units and notable Eocene-Miocene granitic intrusive complexes (Wilson et al., 2015). Late-

86 Pleistocene volcanic activity on southern Kruzof Island formed the Mt. Edgecumbe volcanic

87 field (Riehle, 1996). Post-LLGM (late-Pleistocene and Holocene) eruptions formed extensive

88 andesite flows on the island and blanketed much of the surrounding area with tephra (Riehle et

89 al., 1984; Riehle et al., 1992; Riehle, 1996). Modern climate of the Alexander Archipelago is

90 dominated by cool, wet summers and mild winters, with perennial heavy rainfall - Sitka (Baranof

91 Island) receives ~2200 mm/yr while Chichagof Island receives over 3300 mm/yr (Ager, 2019;

92 https://wrcc.dri.edu/summary/ Climsmak.html). Snowfall is minimal at lower elevations, but

93 more substantial in higher elevation areas (https://wrcc.dri.edu/summary/ Climsmak.html).

94 Glaciers occupy alpine cirques in the Alexander Archipelago (totaling < 150 km^2), primarily on

95 Baranof and Chichagof islands (Molnia, 2008). Presently, low-elevation (< 700 m asl) areas of

96   the archipelago are dominated by coniferous rainforests, while alpine tundra exists above the tree

97   line (> 700 m asl; Ager, 2019).

98   Previous mapping shows much, if not all, of southeast Alaska covered by the Cordilleran

99   Ice Sheet during the LLGM and the last deglaciation, with a maximum position likely

100   terminating several kilometers out on the continental shelf of the Gulf of Alaska (Carrara et al.,

101   2007). Ice caps formed atop the Coast Mountains and high massifs of the Alexander Archipelago

102   coalesced and flowed westward to the continental shelf and the Pacific Ocean (Capps, 1932;

103   Mann, 1986; Mann and Hamilton, 1995). Outlet glaciers occupied the present fjord and strait

104   landscape (Carrara et al., 2007). Today, the landscape is strewn with clear indicators of

105   widespread glaciation including deep fjords, glacially sculpted bedrock draped with boulders,

106   and a variety of other glacial landforms, but it remains unclear whether all of southeast Alaska

107   was covered by the Cordilleran Ice Sheet during the LLGM. Some areas of the Alexander

108   Archipelago, presently above sea level, are hypothesized to have been ice-free throughout the

109   LLGM (Carrara et al., 2007). Recent studies using [10]Be surface exposure dating of glacial

110   landforms, however, indicate that some of these purported ice-age refugia in the southern

111   Alexander Archipelago were covered by the Cordilleran Ice Sheet during its LLGM advance

112   (Lesnek et al., 2018). Other areas previously mapped as ice age refugia in the northern Alexander

113   Archipelago (Carrara et al., 2007; Dalton et al., 2020) are investigated in this study; if their

114   presence is confirmed with numerical dating techniques, this would be a significant confirmation

115   of the existence of coastal refugia.

116

117

3 Methods

3.1 Boulder and bedrock sampling

We collected 29 samples (11 bedrock, 18 boulder) for cosmogenic ^{10}Be surface exposure

dating (hereafter ^{10}Be dating) during summer 2018, 2019, and 2020 (Figs. 3 and 4) from several

sites in coastal Southeast Alaska, including Suemez (n = 4), Baranof (n = 11), Biorka (n = 4),

Kruzof (n = 4) and Chichagof (n = 6) islands. Our samples range in elevation from ~50 to ~930

m asl; all sites are above the local marine limits of ~10 – 20 m asl (Baichtal et al., 2021). We

preferentially sampled paired sites consisting of stable boulders and neighboring unvegetated

bedrock surfaces. This strategy allowed us to assess whether bedrock surfaces contain isotopic

inheritance and provides insights into ice-sheet erosion history. In the absence of suitable

boulders at a few locations, we sampled bedrock with clear evidence of glacial erosion to

mitigate the possibility of ^{10}Be inheritance.

We also collected samples from four glacially-transported boulders on the southwestern

portion of Suemez Island for ^{36}Cl surface exposure dating during the summer 2019 field season

(Figs. 5; 6; Table 2). The boulders consist of non-vesicular olivine basalt of "Tertiary to

Quaternary" age (Eberlein et al.,1983).

Surface samples were collected from the upper few centimeters of the boulders and

bedrock using a handheld angle grinder, hammer, and chisel. We avoided sampling areas of the

boulder tops and bedrock surfaces with visible signs of surface erosion (e.g., fractures,

weathering pits). We did, however, observe erosional features on the boulders sampled for ^{36}Cl

dating. We avoided collecting material from these areas, instead sampling parts of the basaltic

boulder tops that showed fresh, unweathered surfaces. We recorded sample locations with a

142   handheld GPS unit or GAIA GPS (both with a vertical uncertainty of ± 5 m) and measured

143   topographic shielding in the field with a clinometer and compass.

144

145   **3.2 ^{10}Be dating**
146
147   We processed samples at the University at Buffalo Cosmogenic Isotope Laboratory

148   following established quartz purification and beryllium extraction procedures (e.g., Corbett et al.,

149   2016). After quartz purification, we dissolved samples in hydrofluoric acid with precisely

150   weighed ^{9}Be carrier (PRIME Lab 2017.11.17-Be #3/#4; ^{9}Be concentration of 1074 ± 8 ppm). We

151   isolated, oxidized, and packed beryllium into target cathodes in five different batches for

152   accelerator mass spectrometer (AMS) analysis at PRIME lab at Purdue University. The samples

153   were measured with respect to the 07KNSTD standard (^{10}Be/^{9}Be ratio of 2.85 x 10^{-12}; Nishiizumi

154   et al., 2007). We corrected sample ratios using batch-specific blank values between 7.50 x 10^{-16}

155   and 3.14 x 10^{-15}. AMS analytical uncertainty ranged from 3.2 to 7.3% with an average value of

156   4.7%.

157   We calculated all ^{10}Be ages using version 3 of the CRONUS-Earth exposure age

158   calculator (hess.ess.washington.edu; Balco et al., 2008; Balco, 2017), using the Arctic production

159   rate (Young et al., 2013) and a time-dependent (Lm) scaling scheme (Lal, 1991).

160

161   **3.3 ^{36}Cl dating**
162
163   All whole rock samples were prepared at the University of New Hampshire Cosmogenic

164   Isotope Laboratory using a modified version of the protocols in Stone et al. (2000) and Licciardi

165   et al. (2008). After samples were crushed, etched in nitric acid, and homogenized, total sample

166   chloride was measured on a ~1 g aliquot of rock that was spiked with a small amount of 37Cl-

167 enriched solution (LLNL Spike A; 35Cl/37Cl = 0.93; 1285 ± 3 ppm Cl) and a carrier containing

168 ~4000 µg of Br. Cl was extracted as Ag(Cl,Br) following standard procedures and chlorine

169 concentrations were determined through isotope dilution of 35Cl/37Cl ratios (Faure, 1986). 36Cl

170 was extracted from full rock samples as Ag(Cl,Br) after adding a carrier containing ~4800 µg of

171 Br and a natural ratio Cl carrier (35Cl/37Cl = 3.127; 1436 ± 9 ppm Cl) to increase the size of the

172 final precipitate.

173 ^{35}Cl/^{37}Cl and ^{36}Cl/Cl ratios were measured at the Center for Accelerator Mass

174 Spectrometry at Lawrence Livermore National Laboratory. Analytical uncertainty on ^{35}Cl/^{37}Cl

175 measurements ranged from 0.04% to 0.43%; analytical uncertainty on ^{36}Cl/Cl measurements

176 ranged from 2.12% to 2.87%. Major and trace element analyses were conducted by SGS

177 Minerals Services in Burnaby, British Columbia, Canada. Reported total Cl and ^{36}Cl

178 concentrations are corrected for batch-specific process blanks (Table 2). Analytical data used to

179 determine surface exposure ages are provided in supplementary tables S1 and S2. ^{36}Cl exposure

180 ages were calculated using an in-development version of the CRONUS-Earth ^{36}Cl calculator

181 (http://stoneage.ice-d.org/math/Cl36/v3/v3_Cl36_age_in.html) and Lm scaling (Lal, 1991).

182

183 **3.4 Exposure age calculation considerations**
184

185 We made no corrections for post-glacial elevation changes or snow cover when

186 calculating our ^{10}Be and ^{36}Cl ages. Post-glacial isostatic adjustment results in a time-varying rate

187 of cosmogenic nuclide production (Jones et al., 2019). This effect can be corrected for using

188 comprehensive records of regional emergence constrained by glacial isostatic adjustment models

189 or relative sea-level histories. Hundreds of radiocarbon ages constrain the relative sea level

190 chronology in the Alexander Archipelago; the sites in our study experienced ~50 m of relative

191   sea level lowering due to forebulge collapse between ~15 and 10 ka (Baichtal et al., 2021).

192   Corrections for glacial isostatic adjustment history, albeit slightly uncertain given site-to-site

193   differences in elevation history, result in small changes (~1% age decrease), and thus we report

194   our ages without any correction for isostatic adjustment (Tables 1 and 2). Furthermore, changes

195   in air pressure near a retreating ice margin and shifts in air compression above a sample site that

196   experienced elevation change may mitigate any effects of isostatic adjustment on cosmogenic

197   nuclide production, potentially rendering any elevation correction unnecessary (Staiger et al.,

198   2007).

199   Extended periods of thick and dense snow cover can also inhibit ^{10}Be and ^{36}Cl production

200   in a rock surface and lead to erroneously young apparent exposure ages. While modern snowfall

201   reports for lower-elevation areas of the Alexander Archipelago indicate minimal average

202   wintertime snow cover (10 – 20 cm; https://wrcc.dri.edu/summary/ Climsmak.html), there are no

203   data for higher-elevation areas. Consequently, we cannot report our ages with reliable snow

204   shielding corrections and these exposure dates should be considered minimum ages. However,

205   most of our sites are from low to moderate elevations (<500 m asl; Table 1).

206   Post-depositional weathering and erosion can also affect exposure ages. We observed

207   fresh, unweathered glacially scoured bedrock across all our field sites, indicating minimal post-

208   glacial erosion. We made no corrections for erosion in our age calculations presented within the

209   manuscript text and thus these should be considered minimum ages. For sensitivity purposes, we

210   calculated ages using an erosion rate of 0.3 cm/kyr, similar to erosion rates applied nearby in

211   British Columbia (Menounos et al., 2017). These erosion-corrected ages are between 2% and 7%

212   older and are found in Tables S3 and S4.

213   Both cosmogenic and nucleogenic ^{36}Cl can be present in rock surfaces, and for our

214   surface exposure age calculations we assumed steady state production/decay of nucleogenic ^{36}Cl.

215   Moderate amounts of nucleogenic ^{36}Cl are produced when ^{35}Cl absorbs neutrons released by the

216   decay of U and Th isotopes (Gosse and Phillips, 2001). However, because the formation age of

217   the sampled basalt flow on Suemez Island is loosely constrained to the "Tertiary to Quaternary"

218   (Eberlein et al., 1983), nucleogenic ^{36}Cl production/decay may or may not be in steady state. To

219   assess the sensitivity of our exposure ages to the assumption of steady state nucleogenic ^{36}Cl

220   production, we also calculated exposure ages using a rock formation age of 20 ka, which, given

221   the timing of the LLGM ice advance in Southeast Alaska (Lesnek et al., 2018), is the youngest

222   formation age we might expect for these rocks. Results of this test (Table S3) show that

223   calculated ^{36}Cl ages are relatively insensitive to rock formation age (<1% surface exposure age

224   increase in all cases), which is well within total uncertainty.

225

226   **4 Results**
227

228   We sampled from the summit of a massif at ~410 m asl on south-central Suemez Island

229   (southern Alexander Archipelago) and from a flat bench scattered with boulders on the summit's

230   flank for ^{10}Be dating (Fig. 6). The two boulders sampled on the bench date to 15.6 ± 0.7

231   (19SEAK-07; Fig. 3) and 15.0 ± 1.1 ka (19SEAK-08; we report all surface exposure ages with 1

232   σ internal uncertainty; Table 1). The summit site featured fresh glacially sculpted bedrock

233   surfaces with a couple boulders resting on the bedrock. A boulder and its adjacent bedrock

234   surface, as a pair, date to 17.4 ± 1.2 (19SEAK-09) and 19.7 ± 1.2 ka (19SEAK-10), respectively

235   (Fig. 3). The three boulders yield a mean age of 16.0 ± 1.2 ka (n = 3; 1 SD).

236   On southwestern Suemez Island, we sampled four large boulders for ^{36}Cl dating. The

237   boulders were distributed across a terrain of patchy muskeg with locally outcropping bedrock.

238   Based on reconstructed Cordilleran Ice Sheet flow directions (Lesnek et al., 2020) and boulder

239   composition (supplementary table S2; Eberlein et al., 1983), the boulders were likely plucked

240   from basalt flows present on the southwestern portion of Suemez Island (Brew, 1996). The four

241   basalt boulders from southwestern Suemez Island have ^{36}Cl exposure ages ranging from 12.4 ±

242   0.3 to 16.4 ± 0.5 ka (ages are reported at 1 σ internal uncertainty; Fig. 5; Table 2). ^{36}Cl surface

243   exposure ages assuming 3 mm/ka of surface erosion and non-steady state nucleogenic ^{36}Cl

244   production are presented in Table S3; for all four samples, changing these parameters results in

245   calculated surface exposure ages <2% higher than those presented in the main text.

246   We collected samples from four sites (Baranof Sites A – D; Fig. 7) on the ocean-facing

247   side of Baranof Island, northern Alexander Archipelago. Here, we chose our helicopter ground

248   stops in an area previously mapped as ice-free throughout the LLGM (Carrara et al., 2007; Fig.

249   7). Evidence for glacial sculpting of bedrock surfaces is clear; glacial grooves, striations and

250   chatter marks are present at all sites, and the bedrock surfaces, in places, are topped by perched

251   boulders (Fig. 3). Field evidence of recent glaciation, including relatively unweathered chatter

252   marks, grooves, and striations, contradicts prior mapping of these areas being ice-free during the

253   LLGM.

254   Baranof Site A is a large, unforested area of bedrock outcrops composed of several

255   smaller ridges. Here, we sampled two bedrock surfaces – one from the stoss side of a bedrock

256   outcrop (19SEAK-18; Fig. 3) and one from the top surface of a nearby bedrock patch (19SEAK-

257   19) – which date to 21.7 ± 0.9 and 28.0 ± 1.1 ka, respectively. A boulder sampled adjacent to

258   bedrock (sample 19SEAK-18) yielded an exposure age of 16.9 ± 0.8 ka (19SEAK-17). A second

259   boulder sample from this site dates to 14.4 ± 0.7 ka (19SEAK-20; Fig. 3). At Baranof Site B – a

260   raised bedrock knob – we sampled two boulders and one bedrock surface. The two boulders have

261   ^{10}Be ages of 15.1 ± 0.6 ka (19SEAK-23; Fig. 3), 14.4 ± 0.7 ka (19SEAK-21); the bedrock sample

262   has a ^{10}Be age of 14.4 ± 0.6 ka (19SEAK-22). Baranof Site C is a high ridge between the ocean

263   and a U-shaped valley with abundant bedrock outcrops and few boulders. Here, a boulder yielded

264   an exposure age of 16.3 ± 0.6 ka (19SEAK-24; Fig. 3) whereas a bedrock surface dates to 15.7 ±

265   0.6 ka (19SEAK-25). Finally, Baranof Site D is a small bedrock ridge between two peaks with

266   massive stoss and lee features. At this site, we collected samples from two quartz veins in the

267   bedrock, which have exposure ages of 18.2 ± 0.7 (19SEAK-26; Fig. 3) and 20.2 ± 0.8 ka

268   (19SEAK-27). Because the sites are all in relatively close proximity and from similar elevations

269   (50 – 160 m asl), we treat the samples as having experienced the same glacial history, and thus

270   should belong to a single age population. Collectively, boulder samples yield a mean age of 15.4

271   ± 1.1 ka (n = 5; 1 SD) with no obvious outliers, whereas the bedrock samples exhibit more scatter

272   and are mostly older than the mean boulder age (Fig. 9).

273   Biorka Island, a small island off the western coast of central Baranof Island, was initially

274   mapped as ice-covered throughout the LLGM (Dyke, 2004). Here, there are numerous ~1 m tall

275   boulders that rise above the surrounding vegetation and rest on ice-sculpted bedrock. Vegetation

276   and sediments mostly obscure underlying bedrock surfaces, and thus we only collected samples

277   from boulders at this sampling site. Our four boulder samples yielded exposure ages of 15.3 ±

278   0.5 (18JB005; Fig. 4), 14.9 ± 0.6 (18JB006), 15.4 ± 0.5 (18JB007; Fig. 4), and 13.7 ± 0.5 ka

279   18JB008), with a mean of 14.8 ± 0.8 ka (n = 4; 1 SD; Fig. 8).

280   We visited a summit ridge at 545 – 560 m asl on the western, ocean-facing side of

281   northwestern Kruzof Island, previously mapped as ice-free throughout the LGM (Dalton et al.,

282 2020). There, we found many large stable boulders and exposed patches of glacially sculpted

283 bedrock between vegetation exhibiting glacial grooves and chatter marks. Here, we sampled

284 three large boulders (> 2 x 2 x 1 m), which date to 14.9 ± 0.8 (20SEAK-07; Fig. 4), 14.9 ± 0.9

285 (20SEAK-12) and 14.6 ± 0.8 ka (20SEAK-13; Fig. 4), yielding a mean age of 14.8 ± 0.2 ka (n =

286 3; 1 SD; Fig. 8). A bedrock surface at this site dates to 13.4 ± 1.0 ka (20SEAK-10; Fig. 4) and

287 sits ~10 m below and ~10 m away from the boulder that dated to 14.6 ± 0.8 ka (20SEAK-13).

288   We collected samples from three sites on Chichagof Island (Chichagof Sites A – C; Fig.

289 8). Unlike our other sampling locations which are on the ocean-facing, western sides of the

290 archipelago, the Chichagof Island sites are all located inland. We visited these sites to determine

291 the timing of ice retreat inland and to complement the findings of a previous study that

292 documented ice withdrawal in the central and eastern Alexander Archipelago (Lesnek et al.,

293 2020). Chichagof Island is notable for its relative lack of boulders – consequently, the boulders

294 sampled here are smaller than those at other sites. While many bedrock outcrops featured smooth

295 surfaces indicative of glacial erosion, we did not observe clear striations or chatter marks. At site

296 A, a bedrock bench, [10]Be ages from two small, perched boulders are 12.7 ± 0.7 (20SEAK-15; 0.5

297 x 0.3 x 0.3 m; 476 m asl; Fig. 4) and 9.0 ± 0.6 ka (20SEAK-16; 0.5 x 0.4 x 0.3 m; 473 m asl). A

298 quartz vein sampled from bedrock outcrop at this site has an exposure age of 15.3 ± 0.7 ka

299 (20SEAK-14). Site B is a series of bedrock ridges, and a single boulder yields an exposure age of

300 12.4 ± 0.9 ka (20SEAK-18; 817 m asl; Fig. 4), while an adjacent bedrock surface dates to $14.1 \pm$

301 0.7 ka (20SEAK-19; 816 m asl). Finally, site C is at the summit of a massif and one bedrock

302 knob sampled here has an exposure age of 17.7 ± 0.8 ka (20SEAK-22; 779 m asl; Fig. 4).

303

304

305 **5 Discussion**

306

307 **5.1 Bedrock ^{10}Be ages**

308

309   We sampled large and stable boulders in addition to bedrock surfaces with clear evidence

310 of glacial erosion (e.g., striations, chatter marks) with the goal of providing optimal constraints

311 on deglaciation. Sampling bedrock surfaces also allows us to better understand the subglacial

312 erosion regime across the Alexander Archipelago, potentially yielding information about the

313 duration of ice cover, the amount of subglacial erosion, and the likelihood of boulders containing

314 inheritance.

315   Bedrock exposure ages are older than the mean boulder exposure ages by two SD or

316 greater on Suemez Island (19SEAK-10) and Baranof sites A (19SEAK-18, 19SEAK-19) and D

317 (19SEAK26, 19SEAK-27). At Chichagof site A the bedrock exposure age (20SEAK-14) is ~4.5

318 kyr older than the mean boulder age, but still within two standard deviations, perhaps due to the

319 large spread in boulder ages resulting in larger standard deviations. At Chichagof site B, the

320 single boulder ^{10}Be age (20SEAK-18) post-dates the single bedrock age by ~1.7 kyr. In general,

321 bedrock data reported here are consistent with bedrock ^{10}Be ages from Warren and Baker islands

322 that are older (by more than 2 SD) than mean boulder ages (Lesnek et al., 2018). Bedrock ages

323 may be erroneously older due to ^{10}Be inheritance if ice sheet erosion was insufficient to remove

324 the ~2 m of rock required to remove most of the previous ^{10}Be inventory. Studies from British

325 Columbia (Darvill et al., 2018) and Washington (Briner and Swanson, 1998) also report

326 cosmogenic nuclide inheritance in bedrock from other areas covered by the Cordilleran Ice

327 Sheet. In our field area, the short-lived nature of the overriding event (~3 kyr; Lesnek et al.,

328 2018) may also contribute to the lack of significant glacial erosion. Finally, traces of inheritance

329   may be present in bedrock, perhaps even boulders, in ice-sheet-distal sites like these that are

330   overrun by ice during extremely brief portions of the Quaternary (Briner et al., 2016).

331   In some cases, boulder-bedrock pairs have similar exposure ages (on southern Baranof

332   and Suemez islands), suggesting our bedrock ages are unaffected by ^{10}Be inheritance at these

333   sites. On Kruzof Island, a bedrock patch yields an exposure age that is younger (by more than 2

334   σ) than the mean age of the surrounding boulders. Potential cover by snow, sediment, or

335   vegetation is thought to have caused anomalously young ages elsewhere in the Alexander

336   Archipelago (Lesnek et al., 2020) and may also explain this ^{10}Be age from our bedrock site on

337   Kruzof Island.

338   Bedrock exposure ages vary greatly (by as much as ~14 kyr) between the various

339   sampling locations on Baranof Island and up to 6 kyr on Suemez Island (Lesnek et al., 2018).

340   The Alexander Archipelago is characterized by impressive relief (deep fjords, high peaks), and

341   thus, sub-glacial erosion rates clearly varied greatly across Suemez and Baranof islands where

342   sampling locations are ~2 – 6 km apart. Differing bedrock ^{10}Be ages from the same sampling

343   locales confirm this inference, reflecting variable sub-glacial erosion rates even within ~100 m of

344   each other. Some samples may have been collected in areas dominated by glacial abrasion,

345   whereas other samples might be from surfaces dominated by quarrying, and thus, this variability

346   could reflect varying subglacial processes on a local scale.

347   Because bedrock exposure ages from the coastal Alexander Archipelago (this study;

348   Lesnek et al., 2018) do not consistently pre-date, match, or post-date exposure ages from

349   adjacent boulders, we refrain from including bedrock-based ^{10}Be ages in our mean deglaciation

350   age calculations (Figs. 9; 10). This negates biases when choosing which bedrock ages "match"

351   nearby erratic ages and allows us to eliminate any concern over inheritance or post-ice retreat

352   cover of these bedrock surfaces. While bedrock ages, especially when paired with boulder ages,

353   are useful for identifying spatially variable subglacial erosion processes and issues with past

354   cover and inheritance, they do not appear to provide reliable age constraints on the timing of

355   deglaciation in the Alexander Archipelago due to the inconsistencies between bedrock and

356   boulder ages. In light of this, we also recalculate relevant mean ages from Lesnek et al. (2018;

357   2020) using solely boulder ^{10}Be ages to update these other regional chronologies.

358

5.2 ^{10}Be chronology incompatible with mapped Cordilleran Ice Sheet extent

359
360

361   We targeted areas of the northern Alexander Archipelago mapped as ice-free by previous

362   studies to determine whether these areas were LLGM refugia. The most recent coastal

363   Cordilleran Ice Sheet reconstructions show significant portions of the northern Alexander

364   Archipelago as remaining ice-free throughout the LLGM (Fig. 2), with ice terminating close to

365   the present shoreline – not on the continental shelf (Dalton et al., 2020; Lesnek et al., 2020). Our

366   data, however, indicate that at least some of these areas previously mapped as refugia

367   (southwestern Baranof and Kruzof islands) were covered by ice, and deglaciated around 15.4 –

368   14.8 ka. Our new evidence thus suggests that ice extended onto the continental shelf during the

369   LLGM, as in the southern Alexander Archipelago (Lesnek et al., 2018). These discrepancies

370   between previously mapped ice extents and those implied by our new exposure ages highlight

371   the need to develop deglaciation chronologies elsewhere along the Cordilleran Ice Sheet coastal

372   margin to provide updated mapping around the north Pacific.

373

374

5.3 Cordilleran Ice Sheet retreat across the Alexander Archipelago

Mean boulder ^{10}Be exposure ages from Suemez Island in this study and Lesnek et al. (2018), 16. ± 1.2 ka (n = 3 boulders; 1 SD) and 16.6 ± 0.8 ka (n = 3 boulders; 1 SD), respectively, overlap within 1 standard deviation (Figs. 6; 9). However, three of the boulder ^{36}Cl ages from southwestern Suemez Island do not overlap with the ^{10}Be ages at 1 standard deviation (Figs. 6; 9). We attribute this scatter to post-depositional surface erosion of the basaltic boulders (i.e., those dated with 36Cl) in excess of 3 mm/ka. Although we targeted areas of the boulder tops with no obvious signs of erosion, given the maritime climate of Southeast Alaska it is possible that the original, glacially eroded boulder surfaces have been weathered. Surface erosion of rocks with low concentrations of native Cl (supplementary table S2), where the primary ^{36}Cl production pathway is Ca-spallation (Marrero et al., 2016), results in exposure ages that are erroneously young. Thus, we interpret the oldest ^{36}Cl exposure age (16.4 ± 0.5 ka; 19SEAK-02) as the closest constraint on deglaciation at that site. This ^{36}Cl age overlaps with the ^{10}Be ages from elsewhere on Suemez Island; we combine them and calculate a new, boulder-based mean deglaciation age of 16.3 ± 0.8 ka (n = 10 boulders; 1 SD) for Suemez Island.

We group together three of our sampling locations in the northern Alexander Archipelago that are ocean-facing: Kruzof, Biorka, and southern Baranof islands. As the Cordilleran Ice Sheet retreated from the continental shelf inland, these were the first areas presently above sea level to become ice-free. We calculate a mean ^{10}Be boulder age of 15.1 ± 0.9 ka (n = 12 boulders; 1 SD) for the coastal northern Alexander Archipelago.

There are limited data from elsewhere in the northern Alexander Archipelago that constrain the timing of deglaciation. A basal pollen concentrate-based radiocarbon age from Hummingbird Lake (Fig. 7), southwestern Baranof Island dates to 15.0 ± 0.2 cal ka, in

399   agreement with the [10]Be ages presented here and that collectively indicate coastal Baranof Island

400   was deglaciated prior to ~15 ka (Ager, 2019). Additionally, tephra layers from Mt. Edgecumbe

401   on Kruzof Island are dated to 13.1 ka (Riehle et al., 1992; Beget et al., 1998), and blanket many

402   of the surrounding islands, suggesting that these areas were ice-free by then.

403   All three sample sites on Chichagof Island (Sites A – C) are not ocean-adjacent and

404   characterized by a general lack of boulders. The boulders present were much smaller and shorter

405   (< 0.5 m high) than boulders sampled elsewhere across the Alexander Archipelago – we chose to

406   sample these despite their size to provide minimum ages for deglaciation and to compare with

407   available radiocarbon constraints. The ages of these boulders fall between 9.0 ± 0.6 and $12.7 \pm$

408   0.7 ka and are thus younger than other age constraints for deglaciation on Chichagof Island;

409   radiocarbon ages on shells from raised marine terraces on Chichagof Island date back to $14.2 \pm$

410   0.6 cal ka suggesting that the island was ice-free by this time (Baichtal et al., 2021). Smaller

411   boulders are more susceptible to cover (whether snow, vegetation, or sediment), and may thus

412   yield anomalously young [10]Be ages. While a lack of large boulders found on Chichagof Island

413   makes it difficult to ascertain the timing of deglaciation, regional glacial and sea-level history

414   suggests Chichagof Island was deglaciated between 15.1 (when the coastal area deglaciated) and

415   14.2 cal ka (the age of shells in raised marine deposits). Therefore, the boulders dated here likely

416   have anomalously young exposure ages.

417   Our mean [10]Be age of 15.1 ± 0.9 ka (n = 12 boulders; 1 SD) from all sites along the

418   coastal portion of the northern Alexander Archipelago fits with the few other regional

419   deglaciation constraints (Fig. 2) and overlaps within one standard deviation with the mean

420   boulder exposure age from the southern Alexander Archipelago of 16.3 ± 0.8 ka (n = 13

421   boulders; 1 σ; this study; Lesnek et al., 2018; Lesnek et al., 2020). While mean ages from the

422   northern and southern Alexander Archipelago overlap within one standard deviation, it is

423   possible that these areas deglaciated at slightly different times as these various sampling sites

424   happened to become ice-free. Furthermore, local ice caps formed and radiated from massifs on

425   Chichagof, Baranof, and Prince of Wales islands during the LLGM (Capps, 1932; Mann and

426   Hamilton, 1995; Lesnek et al., 2020). These local ice caps served as a local ice source for the

427   Alexander Archipelago and their locations and flow patterns may have led to some parts of the

428   archipelago becoming ice-free before others. Thus, we present a range of deglaciation across the

429   coastal Alexander Archipelago from between 16.3 ± 0.8 ka and 15.1 ± 0.9 ka

430   Ice retreat across the Alexander Archipelago is also registered in marine sediments off

431   the former coastal Cordilleran Ice Sheet margin. Several marine sedimentary records (cores

432   EW0408-26JC, EW0408-66JC, EW0408-85JC) extending back to ~18.5 cal ka show the

433   presence of IRD beginning ~18.5 ka, peaking at 17.5 – 16.5 ka and ceasing at 14.8 ka, reflecting

434   a final retreat of marine-terminating ice (Praetorius and Mix, 2014). Furthermore, these IRD data

435   record fluctuating but relatively elevated calving spanning 18.5 to 14.8 ka, perhaps indicating

436   steady retreat punctuated by periods of accelerated melting.

437   Tephra from Mt. Edgecumbe (Kruzof Island) found in core EW0408-26JC is interpreted

438   to have been deposited in a submarine environment, suggesting that this core site was ice-free by

439   14.6 ka (Praetorius et al., 2016). Records of a subsequent eruption dated to ~13.1 cal ka from

440   marine sediments in Sitka Sound (core EW0408-40JC) indicate that this area (between Baranof

441   and Kruzof islands) must have been ice-free by this time (Addison et al., 2010). Finally, ^{14}C ages

442   from mollusks found in a diamicton layer along the Gastineau Channel date to ~13.8 cal ka,

443   reflecting the beginning of deglaciation near the mainland (Miller, 1973; we calibrate all

444   uncalibrated ^{14}C ages with CALIB 8.2; Stuiver et al., 2021).

5.4 Chronologies of Cordilleran Ice Sheet deglaciation across the North Pacific

Radiocarbon ages from the Cordilleran Ice Sheet margin reflect ice advance from ~20 –
17 ka, near the end of the GLGM at 19 ka. Ages from mammalian fossils in Shuká Káa on Prince
of Wales Island indicate Cordilleran Ice Sheet advance ~20 ka in the Alexander Archipelago
(Lesnek et al., 2018). Directly south of the Alexander Archipelago, on eastern Graham Island
(Haida Gwaii) initial ice advance is dated to 24.1 – 22.5 cal ka with a ^{14}C date from a twig
underlying till (Blaise et al., 1990; Mathewes and Clague, 2017). Along the southwestern
Cordilleran Ice Sheet margin, ice reached its maximum extent until ~17.0 ka in the Puget Sound
area (Porter and Swanson, 1998).

Glacier chronologies from the northeastern Pacific coastline also reflect post-GLGM
retreat. On Sanak Island, tephra near the bottom of a lake sediment core dates deglaciation before
~15.9 ka, broadly synchronous with Cordilleran Ice Sheet withdrawal in the Alexander
Archipelago (Misarti et al., 2012). On Kodiak Island, final LLGM retreat dates to ~15.7 cal ka,
as marked by a ^{14}C age above glacio-tectonically altered sediments (Mann and Peteet, 1994).
Directly north of the Alexander Archipelago, a ^{14}C age from a log found within the Finger
Glacier lateral moraine provides a minimum age of deglaciation at ~14.6 cal ka (Mann, 1986).
Radiocarbon ages from a marine sediment core in Dixon Entrance date maximum Cordilleran Ice
Sheet extent to before ~16.1 cal ka and retreat beginning before ~15.3 cal ka (Barrie and
Conway, 1999). A marine sediment record from Vancouver Sound similarly dates maximum ice
extent to 18.5 ka and retreat of the Cordilleran Ice Sheet onto the mainland by 16.4 ka (Blaise et
al., 1990). Quaternary sediments on eastern Graham Island indicate the Cordilleran Ice Sheet was
retreating by 17.8 cal ka (Blaise et al., 1990). Notably, [10]Be ages on Calvert Island suggest ice

468   retreated off the continental shelf at ~18 ka, pre-dating ice withdrawal onto land in the Alexander

469   Archipelago (Darvill et al., 2018).

470   Marine sediment cores are interpreted to show ice retreat across the coastal northeastern

471   Pacific. A marine sediment core (SO202-27-6) from the Gulf of Alaska captures a decrease in

472   sea surface salinity ~16 ka, interpreted to reflect increased meltwater from the Cordilleran Ice

473   Sheet margin (Maier et al., 2018). Another marine sediment core (EW0408-85JC) recovered off

474   the coast of southern Alaska records a decrease in glacial-margin sediment accumulation at 16.9

475   ka as ice stagnated or began to retreat. (Davies et al., 2011). Reductions in salinity captured by

476   planktonic $\delta^{18}O$ in this core at ~16.7 ka are interpreted as an increase in meltwater input from

477   retreating glaciers. A transition from ice-proximal to laminated hemipelagic sediments at ~14.8

478   ka marks glacier retreat off the continental shelf and onto land. Off the coast of Alaska, a marine

479   sediment core records a peak of IRD deposition peaking between 18 and 17 ka, interpreted as the

480   retreat of marine-terminating margins of the Cordilleran Ice Sheet (Walczak et al., 2020).

481   Additionally, another core from off Vancouver Island (MD02-2496) captures IRD deposition

482   between ~17.0 and ~16.2 cal ka – indicating rapid regional deglaciation – and a minor IRD event

483   at ~14.7 cal ka (Cosma et al., 2008).

484   Our new data showing ice retreat at 15.1 ± 0.9 ka from the northern Alexander

485   Archipelago, along with ages of deglaciation from the southern Alexander Archipelago (16.3 ±

486   0.8 ka; this study; Lesnek et al., 2018), are broadly synchronous with previously published ice

487   retreat chronologies for the marine-terminating Cordilleran Ice Sheet margin elsewhere along the

488   northeast Pacific Coast. However, while our chronology only documents deglaciation, it provides

489   further evidence of a delayed LLGM across the coastal Cordilleran Ice Sheet compared to the

490   GLGM maximum extents of alpine glaciers in mainland Alaska (Briner et al., 2017), parts of

491   southern Alaska (Reger et al., 1996), and the Laurentide Ice Sheet (Dalton et al., 2020).

492

493   5.5 Paleoclimate Records from the North Pacific
494

495   Several paleoclimate records from around the North Pacific span our interval of

496   Cordilleran Ice Sheet deglaciation in the Alexander Archipelago. A combined diatom

497   assemblage- and alkenone-derived record of sea surface temperatures (SSTs) from the Bering

498   Sea (Core 51JPC), records perennial sea ice from ~22.5 ka (beginning of record) to 17 ka, and

499   increased SSTs beginning ~16.9 ka before a notable shift back to annual sea ice ~16.7 ka

500   (Caissie et al., 2010). In the northern Gulf of Alaska (Core EW0408-85JC), $\delta^{18}O$ data document

501   increasing SSTs at 16.7 ka and again at ~14.7 ka (Davies et al., 2011). Alkenone-inferred paleo-

502   SST reconstructions from this same core show the lowest SSTs (~5 °C) circa 17.0 ka, with

503   increased SSTs beginning ~16.5 ka, and a rapid ~3 - 4 °C rise in SSTs from 15.2 to 14.7 ka

504   (Praetorius et al., 2015). Alkenone-inferred SST and $\delta^{18}O$ records from the Gulf of Alaska also

505   record increased SSTs of ~3°C at 14.7 ka (cores EW0408-26JC, EW0408-66JC; Praetorius et al.,

506   2016). Off Vancouver Island, Mg/Ca temperature reconstructions from subsurface-dwelling *N.*

507   *pachyderma* indicate two stages of warming of !2 °C at 17.2 – 16 ka, and a further ~3 °C 15.5 –

508   14.0 ka, while surface-dwelling *G. bulloides* record a 3 °C SST increase from 15.0 – 14.0 ka

509   (core MD02-2496; Taylor et al., 2014), all within the uncertainty of coastal Alexander

510   Archipelago ice retreat. Alkenone SST reconstructions from another nearby core (core JT96-09)

511   also indicates a 4 °C increase in SST at ~14.7 ka (Kienast and McKay, 2001).

512   There are few terrestrial paleoclimate data that span the last deglacial period from

513   southeast Alaska and coastal British Columbia. Cordilleran ice cover until ~15 ka across much of

514   the region impeded the preservation of many terrestrial records – however, there are limited ice

515   core, speleothem, and lake records that date back to early regional deglaciation or prior.. A

516   growth hiatus in a speleothem from El Capitan Cave (southern Alexander Archipelago) spanning

517   ~41.5 to ~13.4 ka suggests the cave was either overridden by the Cordilleran Ice Sheet,

518   experienced permafrost conditions and a mean annual air temperature < 0 °C, or lacked drip

519   water (Wilcox et al., 2019). The youngest date also serves as a minimum limit on deglaciation, as

520   the area was thawed by ~13.4 ka. However, El Capitan Cave is ~60 km inland of the outermost

521   coastal region and therefore may have still experienced these conditions while the outer coast

522   deglaciated. At Hummingbird Lake, southwestern Baranof Island, pollen records indicate *Pinus*

523   *contorta* dominated from ~15.2 ka to 14 ka, which is interpreted to represent *Pinus contorta*

524   response to the beginnings of Gulf of Alaska ocean warming at ~16.5 ka (Praetorius et al., 2015;

525   Ager, 2019). This record suggests increased air temperatures around deglaciation of the

526   Alexander Archipelago between 16.3 ± 0.8 ka and 15.1 ± 0.9 ka.

527

528   **5.6 Implications for early human migration**
529

530   Several studies have scrutinized potential areas of LLGM glacial refugia in the Alexander

531   Archipelago through a human migration perspective (Carrara et al., 2007; Lesnek et al., 2018),

532   building off similar approaches from elsewhere in the North Pacific (e.g., Warner et al., 1982;

533   Mann and Peteet, 1994; Misarti et al., 2012). Our study focused on southern Baranof and Kruzof

534   islands because previous mapping suggested that parts of these areas were ice-free throughout

535   the LLGM (Carrara et al., 2003; Carrara et al., 2007). However, our [10]Be ages from southern

536   Baranof Island indicate these areas were glaciated throughout the LLGM and not available for

537   human habitation between ~20 ka and ~15.4 ka. Our exposure ages from Kruzof Island also

538   suggest this area was not ice free until ~14.8 ka.

539   These results indicate that some of the last major unevaluated areas of possible refugia

540   presently above sea-level were covered by ice during the LLGM. At its maximum extent, ice

541   likely extended onto the then-exposed continental shelf. Ice occupation of the continental shelf –

542   or at least parts of the shelf – off the Alexander Archipelago was relatively brief, from ~20.0 to

543   ~16.0 ka (Lesnek et al., 2018). Areas of the continental shelf would have been above modern sea

544   level during this time and until ~11 – 8 ka, when sea level neared modern levels in the Alexander

545   Archipelago (Baichtal et al., 2021). At a minimum, ice lobes would have existed within the

546   major shelf troughs (e.g., Chatham Strait), likely crossing the entire shelf at these locations; at a

547   maximum, the entire continental shelf may have been occupied by ice from ~20 to ~16 ka.

548   Whether portions of the shelf remained ice-free during the LLGM is unknown, but it is possible.

549   Based on the immediate colonization of *Pinus* at 15.2 ka in Hummingbird Lake and as early as

550   ~15.4 ka on Pleasant Island, there were likely ice-free areas on the shelf throughout the LLGM

551   (Hansen and Engstrom, 1996; Ager, 2019).

552

553   **6 Conclusions**
554
555   We conclude that several areas in southeast Alaska previously mapped as ice-free

556   through the LLGM were covered by ice until between ~16.3 and ~15.1 ka. [10]Be ages from

557   boulders suggest that the northern coastal Alexander Archipelago deglaciated at 15.1 ± 0.9 ka,

558   while [10]Be and [36]Cl ages date ice retreat in the southern portion at 16.3 ± 0.8 ka, following a

559   LLGM that began after ~20 ka (Lesnek et al., 2018; Lesnek et al., 2020) The timing of

560   deglaciation in the Alexander Archipelago is similar to some other sites around the Cordilleran

561 Ice Sheet coastal margin (e.g., Mann and Peteet, 1994; Misarti et al., 2012), but later than other

562 locations (e.g., Darvill et al., 2018). Notably, the deglaciation in southeast Alaska is later than in

563 mainland Alaska and Kodiak and Sanak Islands, Alaska (Fig. 1), where records are more aligned

564 with the GLGM. The timing of deglaciation in the Alexander Archipelago is broadly

565 synchronous with regional records of local ocean and air temperature increases. We also found

566 that anomalously old ^{10}Be ages of bedrock surfaces are likely due to inheritance caused by

567 insufficient ice sheet erosion, and thus urge caution when using ages from bedrock surfaces as

568 direct constraints on ice retreat without additional boulder ages along the coastal margins of the

569 Cordilleran Ice Sheet.

570   Our data indicate that previous mapping of the coastal Cordilleran Ice Sheet can be

571 spatially and temporally improved. We suggest that ice likely extended out on the continental

572 shelf along the Alexander Archipelago. We are increasingly confident that areas of the coastal

573 Cordilleran Ice Sheet previously mapped as ice-free throughout the LLGM were in fact covered

574 by ice, and that refugia, if any existed, would have been located on the exposed continental shelf.

575 Although more logistically challenging, subsequent studies should evaluate the existence of

576 LLGM refugia in the Alexander Archipelago by focusing on the previously exposed continental

577 shelf. Special attention should be given to the northern Alexander Archipelago where ice masses

578 were fed by local ice caps and thus may not have been as extensive, as opposed to elsewhere in

579 the northeastern Pacific where ice was sourced from the main body of the Cordilleran Ice Sheet.

580

581 **7 Acknowledgements**

582

583   We acknowledge that these samples were collected on the ancestral lands of the Tlingit

584 and that the University at Buffalo exists on the land of the Seneca. These peoples are the

585   traditional caretakers of these lands and we give thanks for the opportunity to exist and work on

586   lands that are rightfully theirs. We thank the Tongass National Forest for assistance with

587   permitting and logistics. We thank Corey Krabbenhoft, Joseph Tulenko and Karlee Prince for

588   field assistance and Joseph Tulenko and Chris Sbarra for lab assistance. We also thank PRIME

589   Lab for ^{10}Be measurements and Lawrence Livermore National Laboratory for ^{36}Cl

590   measurements. This research was funded by NSF (award # 1854550), the National Geographic

591   Society (award # 57989R-19), a Geological Society of America Student Research Grant (grant

592   number 13631) funded by NSF (award # 1949901), the Alaska Geological Society, and the Mark

593   Diamond Research Fund of the Graduate Student Association at the University at Buffalo, the

594   State University of New York.

595

8 Author Contributions

597   JPB designed the study framework and acquired the majority of grant funds. CKW acquired

598   supplementary funding for fieldwork and lab analyses. CKW, JPB, JFB, and AJL collected

599   samples in the field. CKW conducted ^{10}Be work and AJL and JML performed ^{36}Cl chemistry.

600   CKW, JPB, AJL, and JML analyzed sample data and calculated ages. All authors were involved

601   in interpreting the data. CKW wrote the first draft of the manuscript; all authors provided

602   substantial input. CKW and AJL created figures and tables.

603
604
605
606
607

9 References

Addison, J. A., Beget, J. E., Ager, T. A., and Finney, B. P.: Marine tephrochronology of the Mt. Edgecumbe volcanic field, southeast Alaska, USA, Quaternary Research, 73, 277-292, 2010.

Ager, T. A.: Late Quaternary vegetation development following deglaciation of northwestern Alexander Archipelago, Alaska, Frontiers in Earth Science, 7, 104, 2019.

Baichtal, J. F., Lesnek, A. J., Carlson, R. J., Schmuck, N., Smith, J. L., Landwehr, D. J., and Briner, J. P.: Late Pleistocene and Early Holocene Sea level History Glacial Retreat Interpreted from Shell-bearing Marine Deposits of Southeastern Alaska, GSA Geosphere, 2021.

Balco, G., Stone, J. O., Lifton, N. A., and Dunai, T. J.: A complete and easily accessible means of calculating surface exposure ages or erosion rates from 10Be and 26Al measurements, Quaternary Geochronology, 3, 174-195, https://doi.org/10.1016/j.quageo.2007.12.001, 2008.

Balco, G.: Production rate calculations for cosmic-ray-muon-produced 10Be and 26Al benchmarked against geological calibration data, Quaternary Geochronology, 39, 150-173, 2017.

Barrie, J. V., and Conway, K. W.: Late Quaternary glaciation and postglacial stratigraphy of the northern Pacific margin of Canada, Quaternary Research, 51, 113-123, 1999.

Begét, J. E. and Motyka, R. J.: New dates on late Pleistocene dacitic tephra from the Mount Edgecumbe volcanic field, southeastern Alaska, Quaternary Research, 49, 123-125, 1998.

Blaise, B., Clague, J. J., and Mathewes, R. W.: Time of maximum Late Wisconsin glaciation, West Coast of Canada, Quaternary Research, 34, 282-295, https://doi.org/10.1016/0033-5894(90)90041-I, 1990.

Booth, D. B., Troost, K. G., Clague, J. J., and Waitt, R. B.: The Cordilleran ice sheet, Developments in Quaternary Sciences, 1, 17-43, 2003.

Borchers, B., Marrero, S., Balco, G., Caffee, M., Goehring, B., Lifton, N., Nishiizumi, K., Phillips, F., Schaefer, J., and Stone, J. J. Q. G.: Geological calibration of spallation production rates in the CRONUS-Earth project, 31, 188-198, 2016.

Brew, David A.: Geologic map of the Craig, Dixon Entrance, and parts of the Ketchikan and Prince Rupert quadrangles, Southeastern Alaska, No. 95-215, 1995.

Briner, J. P., and Swanson, T. W.: Using inherited cosmogenic 36Cl to constrain glacial erosion rates of the Cordilleran ice sheet, Geology, 26, 3-6, 1998.

Briner, J. P., Goehring, B. M., Mangerud, J., and Svendsen, J. I.: The deep accumulation of 10Be at Utsira, southwestern Norway: implications for cosmogenic nuclide exposure dating in peripheral ice sheet landscapes, Geophysical Research Letters, 43, 9121-9129, 2016.

Briner, J. P., Tulenko, J. P., Kaufman, D. S., Young, N. E., Baichtal, J. F., and Lesnek, A.: The last deglaciation of Alaska, Cuadernos de investigación geográfica/Geographical Research Letters, 429-448, 2017.

Caissie, B. E., Brigham-Grette, J., Lawrence, K. T., Herbert, T. D., and Cook, M. S.: Last Glacial Maximum to Holocene sea surface conditions at Umnak Plateau, Bering Sea, as inferred from diatom, alkenone, and stable isotope records, Paleoceanography, 25, 2010.

Capps, S. R.: Glaciation in Alaska, 2330-7102, 1932.

652 Carrara, P. E., Ager, T. A., Baichtal, J. F., and VanSistine, D. P.: Map of glacial limits and
653   possible refugia in the southern Alexander Archipelago, Alaska, during the late
654   Wisconsin glaciation, Report 2424, 2003.
655 Carrara, P. E., Ager, T. A., and Baichtal, J. F.: Possible refugia in the Alexander Archipelago of
656   southeastern Alaska during the late Wisconsin glaciation, Canadian Journal of Earth
657   Sciences, 44, 229-244, 10.1139/e06-081, 2007.
658 Cook, J. A., Bidlack, A. L., Conroy, C. J., Demboski, J. R., Fleming, M. A., Runck, A. M.,
659   Stone, K. D., and MacDonald, S. O.: A phylogeographic perspective on endemism in the
660   Alexander Archipelago of southeast Alaska, Biological Conservation, 97, 215-227,
661   https://doi.org/10.1016/S0006-3207(00)00114-2, 2001.
662 Corbett, L. B., Bierman, P. R., and Rood, D. H.: An approach for optimizing in situ cosmogenic
663   10Be sample preparation, Quaternary Geochronology, 33, 24-34,
664   https://doi.org/10.1016/j.quageo.2016.02.001, 2016.
665 Cosma, T. N., Hendy, I. L., and Chang, A. S.: Chronological constraints on Cordilleran Ice Sheet
666   glaciomarine sedimentation from core MD02-2496 off Vancouver Island (western
667   Canada), Quaternary Science Reviews, 27, 941-955,
668   https://doi.org/10.1016/j.quascirev.2008.01.013, 2008.
669 Dalton, A. S., Margold, M., Stokes, C. R., Tarasov, L., Dyke, A. S., Adams, R. S., Allard, S.,
670   Arends, H. E., Atkinson, N., and Attig, J. W.: An updated radiocarbon-based ice margin
671   chronology for the last deglaciation of the North American Ice Sheet Complex,
672   Quaternary Science Reviews, 234, 106223, 2020.
673 Darvill, C. M., Menounos, B., Goehring, B. M., Lian, O. B., and Caffee, M. W.: Retreat of the
674   western Cordilleran ice sheet margin during the last deglaciation, Geophysical Research
675   Letters, 45, 9710-9720, 2018.
676 Davies, M. H., Mix, A. C., Stoner, J. S., Addison, J. A., Jaeger, J., Finney, B., and Wiest, J.: The
677   deglacial transition on the southeastern Alaska Margin: Meltwater input, sea level rise,
678   marine productivity, and sedimentary anoxia, Palaeogeography and Palaeoclimatology,
679   26, 10.1029/2010pa002051, 2011.
680 Demboski, J. R., Stone, K. D., and Cook, J. A.: Further perspectives on the Haida Gwaii glacial
681   refugium, Evolution, 53, 2008-2012, 10.1111/j.1558-5646.1999.tb04584.x, 1999.
682 Dyke, A. S.: An outline of North American deglaciation with emphasis on central and northern
683   Canada, Developments in quaternary sciences, 2, 373-424, 2004.
684 Eberlein, G. D., Churkin, M., Carter, C., Berg, H., and Ovenshine, A.: Geology of the Craig
685   quadrangle, Alaska, US Geological Survey, 2331-1258, 1983.
686 Faure, G.: Isotope systematics in two-component mixtures, Principles of isotope geology, 141-
687   153, 1986.
688 Gosse, J. C., and Phillips, F. M.:. Terrestrial in situ cosmogenic nuclides: theory and application.
689   Quaternary Science Reviews, 20, 1475-1560, 2001.
690 Gregoire, L. J., Otto-Bliesner, B., Valdes, P. J., and Ivanovic, R.: Abrupt Bølling warming and
691   ice saddle collapse contributions to the Meltwater Pulse 1a rapid sea level rise,
692   Geophysical research letters, 43, 9130-9137, 2016.
693 Hansen, B. C. S., and Engstrom, D. R.: Vegetation history of Pleasant Island, southeastern
694   Alaska, since 13,000 yr BP, Quaternary Research, 46, 161-175, 1996.
695 Hebda, C. F. G., McLaren, D., Mackie, Q., Fedje, D., Pedersen, M. W., Willerslev, E., Brown,
696   K.J., and Hebda, R. J.: Late Pleistocene palaeoenvironments and a possible glacial
697   refugium on northern Vancouver Island, Canada: Evidence for the viability of early

698   human settlement on the northwest coast of North America, Quaternary Science Reviews,
699   279, 107388, 2022.
700 Ivanovic, R. F., Gregoire, L. J., Wickert, A. D., Valdes, P. J., and Burke, A.: Collapse of the
701   North American ice saddle 14,500 years ago caused widespread cooling and reduced
702   ocean overturning circulation, Geophysical Research Letters, 44, 383-392, 2017.
703 Jones, R. S., Whitehouse, P. L., Bentley, M. J., Small, D., and Dalton, A. S.: Impact of glacial
704   isostatic adjustment on cosmogenic surface-exposure dating, Quaternary Science
705   Reviews, 212, 206-212, 2019.
706 Kienast, S. S., and McKay, J. L.: Sea surface temperatures in the subarctic northeast Pacific
707   reflect millennial-scale climate oscillations during the last 16 kyrs, Geophysical Research
708   Letters, 28, 1563-1566, 2001.
709 Lal, D.: Cosmic ray labeling of erosion surfaces: in situ nuclide production rates and erosion
710   models, Earth and Planetary Science Letters, 104, 424-439, 1991.
711 Lesnek, A. J., Briner, J. P., Lindqvist, C., Baichtal, J. F., and Heaton, T. H.: Deglaciation of the
712   Pacific coastal corridor directly preceded the human colonization of the Americas,
713   Science Advances, 4, 2018.
714 Lesnek, A. J., Briner, J. P., Baichtal, J. F., and Lyles, A. S.: New constraints on the last
715   deglaciation of the Cordilleran Ice Sheet in coastal Southeast Alaska, Quaternary
716   Research, 96, 140-160, 2020.
717 Maier, E., Zhang, X., Abelmann, A., Gersonde, R., Mulitza, S., Werner, M., Méheust, M., Ren,
718   J., Chapligin, B., and Meyer, H.: North Pacific freshwater events linked to changes in
719   glacial ocean circulation, Nature, 559, 241-245, 2018.
720 Mann, D. H.: Wisconsin and Holocene glaciation of southeast Alaska, 1986.
721 Mann, D. H., and Peteet, D. M.: Extent and Timing of the Last Glacial Maximum in
722   Southwestern Alaska, Quaternary Research, 42, 136-148,
723   https://doi.org/10.1006/qres.1994.1063, 1994.
724 Mann, D. H., and Hamilton, T. D.: Late Pleistocene and Holocene Paleoenvironments of the
725   Pacific Coast, Quaternary Science Reviews, 14, 449-471, 10.1016/0277-3791(95)00016-
726   i, 1995.
727 Marrero, S.M., Phillips, F.M., Caffee, M.W. and Gosse, J.C.,: CRONUS-Earth cosmogenic ^{36}Cl
728   calibration. Quaternary Geochronology, 31, 199-219, 2016.
729 Menounos, B., Goehring, B. M., Osborn, G., Margold, M., Ward, B., Bond, J., Clarke, G. K. C.,
730   Clague, J. J., Lakeman, T., Koch, J., Caffee, M. W., Gosse, J., Stroeven, A. P., Seguinot,
731   J., and Heyman, J.: Cordilleran Ice Sheet mass loss preceded climate reversals near the
732   Pleistocene Termination, Science, 358, 781, 10.1126/science.aan3001, 2017.
733 Mathewes, R. W., and Clague, J. J.: Paleoecology and ice limits of the early Fraser glaciation
734   (Marine Isotope Stage 2) on Haida Gwaii, British Columbia, Canada, Quaternary
735   Research, 88, 277-292, 10.1017/qua.2017.36, 2017.
736 Miller, R. D.: Gastineau channel formation: a composite glaciomarine deposit near Juneau,
737   Alaska, US Government Printing Office, 1973.
738 Misarti, N., Finney, B. P., Jordan, J. W., Maschner, H. D. G., Addison, J. A., Shapley, M. D.,
739   Krumhardt, A., and Beget, J. E.: Early retreat of the Alaska Peninsula Glacier Complex
740   and the implications for coastal migrations of First Americans, Quaternary Science
741   Reviews, 48, 1-6, https://doi.org/10.1016/j.quascirev.2012.05.014, 2012.
742 Molnia, B. F.: Glaciers of North America-Glaciers of Alaska, Geological Survey (US), 2008.

743 Nishiizumi, K., Imamura, M., Caffee, M. W., Southon, J. R., Finkel, R. C., and McAninch, J.:
744   Absolute calibration of 10Be AMS standards, Nuclear Instruments and Methods in
745   Physics Research Section B: Beam Interactions with Materials and Atoms, 258, 403-413,
746   https://doi.org/10.1016/j.nimb.2007.01.297, 2007.
747 Porter, S. C., and Swanson, T. W.: Radiocarbon age constraints on rates of advance and retreat of
748   the Puget lobe of the Cordilleran ice sheet during the last glaciation, Quaternary
749   Research, 50, 205-213, 1998.
750 Praetorius, S. K., and Mix, A. C.: Synchronization of North Pacific and Greenland climates
751   preceded abrupt deglacial warming, Science, 345, 444-448, 2014.
752 Praetorius, S. K., Mix, A. C., Walczak, M. H., Wolhowe, M. D., Addison, J. A., and Prahl, F. G.:
753   North Pacific deglacial hypoxic events linked to abrupt ocean warming, Nature, 527,
754   362-366, 2015.
755 Praetorius, S., Mix, A., Jensen, B., Froese, D., Milne, G., Wolhowe, M., Addison, J., and Prahl,
756   F.: Interaction between climate, volcanism, and isostatic rebound in Southeast Alaska
757   during the last deglaciation, Earth and Planetary Science Letters, 452, 79-89, 2016.
758 Reger, R. D., Pinney, D. S., Burke, R. M., and Wiltse, M. A.: Catalog and initial analyses of
759   geologic data related to middle to late Quaternary deposits, Cook Inlet region, Alaska,
760   State of Alaska Division of Geological and Geophysical Surveys Report of
761   Investigations, 95-96, 1996.
762 Riehle, J. R., Brew, D. A., Reed, K. M., and Bartsch-Winkler, S.: Explosive latest Pleistocene (?)
763   and Holocene activity of the Mount Edgecumbe volcanic field, Alaska, US Geological
764   Survey Circular, 939, 111-114, 1984.
765 Riehle, J. R., Champion, D. E., Brew, D. A., and Lanphere, M. A.: Pyroclastic deposits of the
766   Mount Edgecumbe volcanic field, southeast Alaska: eruptions of a stratified magma
767   chamber, Journal of volcanology and geothermal research, 53, 117-143, 1992.
768 Riehle, J. R.: The Mount Edgecumbe Volcanic Field: A Geologic History, US Department of
769   Agriculture, Forest Service, Alaska Region, 1996.
770 Seguinot, J., Khroulev, C., Rogozhina, I., Stroeven, A. P., and Zhang, Q.: The effect of climate
771   forcing on numerical simulations of the Cordilleran ice sheet at the Last Glacial
772   Maximum, The Cryosphere, 8, 1087-1103, 2014.
773 Seguinot, J., Rogozhina, I., Stroeven, A. P., Margold, M., and Kleman, J.: Numerical simulations
774   of the Cordilleran ice sheet through the last glacial cycle, The Cryosphere, 10, 639-664,
775   2016.
776 Shafer, A. B., Cullingham, C. I., Cote, S. D., and Coltman, D. W.: Of glaciers and refugia: a
777   decade of study sheds new light on the phylogeography of northwestern North America,
778   Mol Ecol, 19, 4589-4621, 10.1111/j.1365-294X.2010.04828.x, 2010.
779 Shafer, A. B. A., White, K. S., Côté, S. D., and Coltman, D. W.: Deciphering translocations from
780   relicts in Baranof Island mountain goats: is an endemic genetic lineage at risk?,
781   Conservation Genetics, 12, 1261-1268, 10.1007/s10592-011-0227-8, 2011.
782 Shakun, J. D., Clark, P. U., He, F., Marcott, S. A., Mix, A. C., Liu, Z., Otto-Bliesner, B.,
783   Schmittner, A., and Bard, E.: Global warming preceded by increasing carbon dioxide
784   concentrations during the last deglaciation, Nature, 484, 49-54, 2012.
785 Spratt, R. M., and Lisiecki, L. E.: A Late Pleistocene sea level stack, Climate of the Past, 12,
786   1079-1092, 2016.

787 Staiger, J., Gosse, J., Toracinta, R., Oglesby, B., Fastook, J., and Johnson, J. V.: Atmospheric
788   scaling of cosmogenic nuclide production: climate effect, Journal of Geophysical
789   Research: Solid Earth, 112, 2007.
790 Stuiver, M., Reimer, P.J., and Reimer, R.W., CALIB 8.2, http://calib.org, 2021.
791 Tarasov, L., Dyke, A. S., Neal, R. M., and Peltier, W. R.: A data-calibrated distribution of
792   deglacial chronologies for the North American ice complex from glaciological modeling,
793   Earth and Planetary Science Letters, 315-316, 30-40,
794   https://doi.org/10.1016/j.epsl.2011.09.010, 2012.
795 Taylor, M. A., Hendy, I. L., and Pak, D. K.: Deglacial ocean warming and marine margin retreat
796   of the Cordilleran Ice Sheet in the North Pacific Ocean, Earth and Planetary Science
797   Letters, 403, 89-98, 10.1016/j.epsl.2014.06.026, 2014.
798 Warner, B. G., Mathewes, R. W., and Clague, J. J.: Ice-free conditions on the Queen Charlotte
799   Islands, British Columbia, at the height of late Wisconsin glaciation, Science, 218, 675-
800   677, 1982.
801 Wilcox, P. S., Dorale, J. A., Baichtal, J. F., Spotl, C., Fowell, S. J., Edwards, R. L., and Kovarik,
802   J. L.: Millennial-scale glacial climate variability in Southeastern Alaska follows
803   Dansgaard-Oeschger cyclicity, Sci Rep, 9, 7880, 10.1038/s41598-019-44231-1, 2019.
804 Wilson, F. H., Hults, C. P., Mull, C. G., and Karl, S. M.: Geologic map of Alaska, US
805   Department of the Interior, US Geological Survey, 2015.
806 Young, N. E., Schaefer, J. M., Briner, J. P., and Goehring, B. M.: A [10]Be production-rate
807   calibration for the Arctic, Journal of Quaternary Science, 28, 515-526, 2013.

808

809

810

811

812

813

814

815

816

817

818

819

820

821

822

Figures and Tables
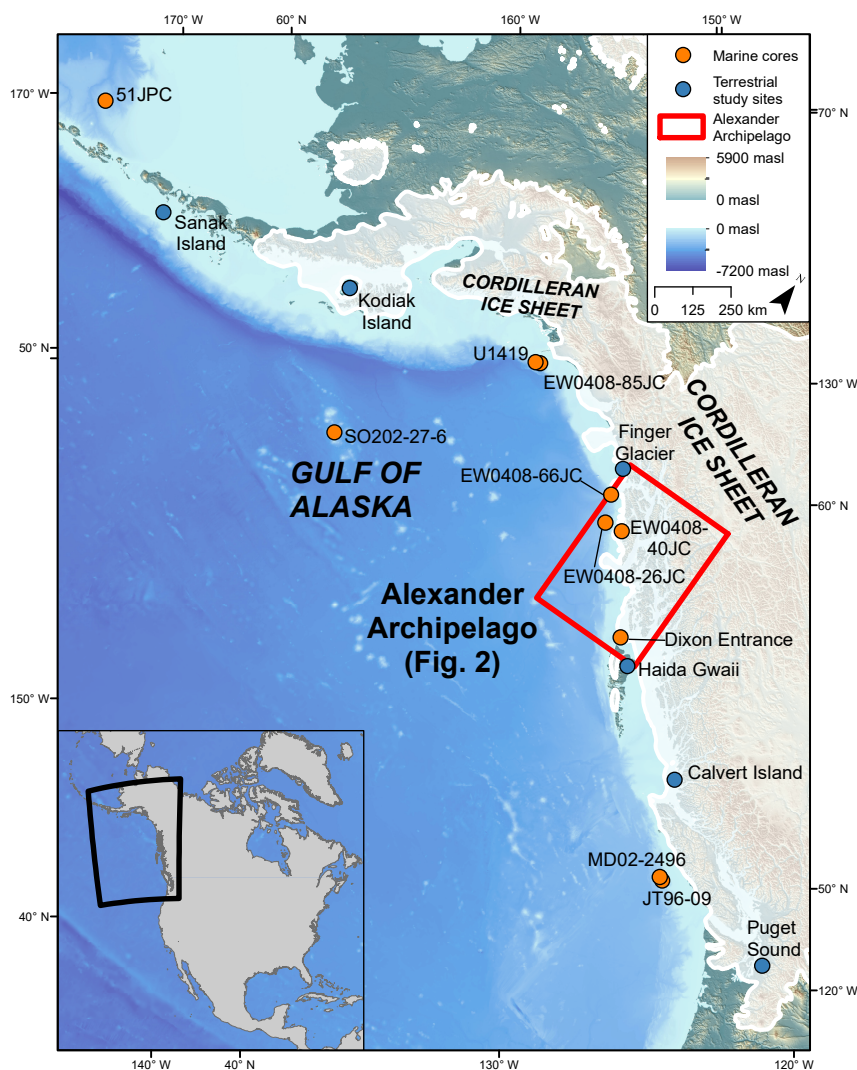
Figure 1: Map of the north Pacific region showing ice limits at 18.0 ka from Dalton et al. (2020) with location of relevant sites mentioned in the text. The Alexander Archipelago is highlighted by the red box on the main figure. Orange dots indicate locations of marine sediment cores: 51-JPC (Caissie et al., 2010), SO202-27-6 (Maier et al., 2018), U1419 (Walczak et al., 2020), EW0408-85JC (Davies et al., 2011; Praetorius and Mix, 2014, Praetoruis et al., 2015), EW0408-66JC (Praetorius and Mix, 2014; Praetorius et al., 2016), EW0408-26JC (Praetorius and Mix, 2014; Praetorius et al., 2016), EW0408-40JC (Addison et al., 2010), MD02-2496 (Cosma and Hendy, 2008), and JT96-09 (Kienast and McKay, 2001). Blue dots indicate location of terrestrial study sites: Sanak Island (Misarti et al., 2012), Kodiak Island (Mann and Peteet, 1994), Finger Glacier (Mann 1986), Haida Gwaii (Clague et al.,1982; Mathewes and Clague, 1982), Calvert Island, (Darvill et al., 2018), and Puget Sound (Porter and Swanson, 1998).
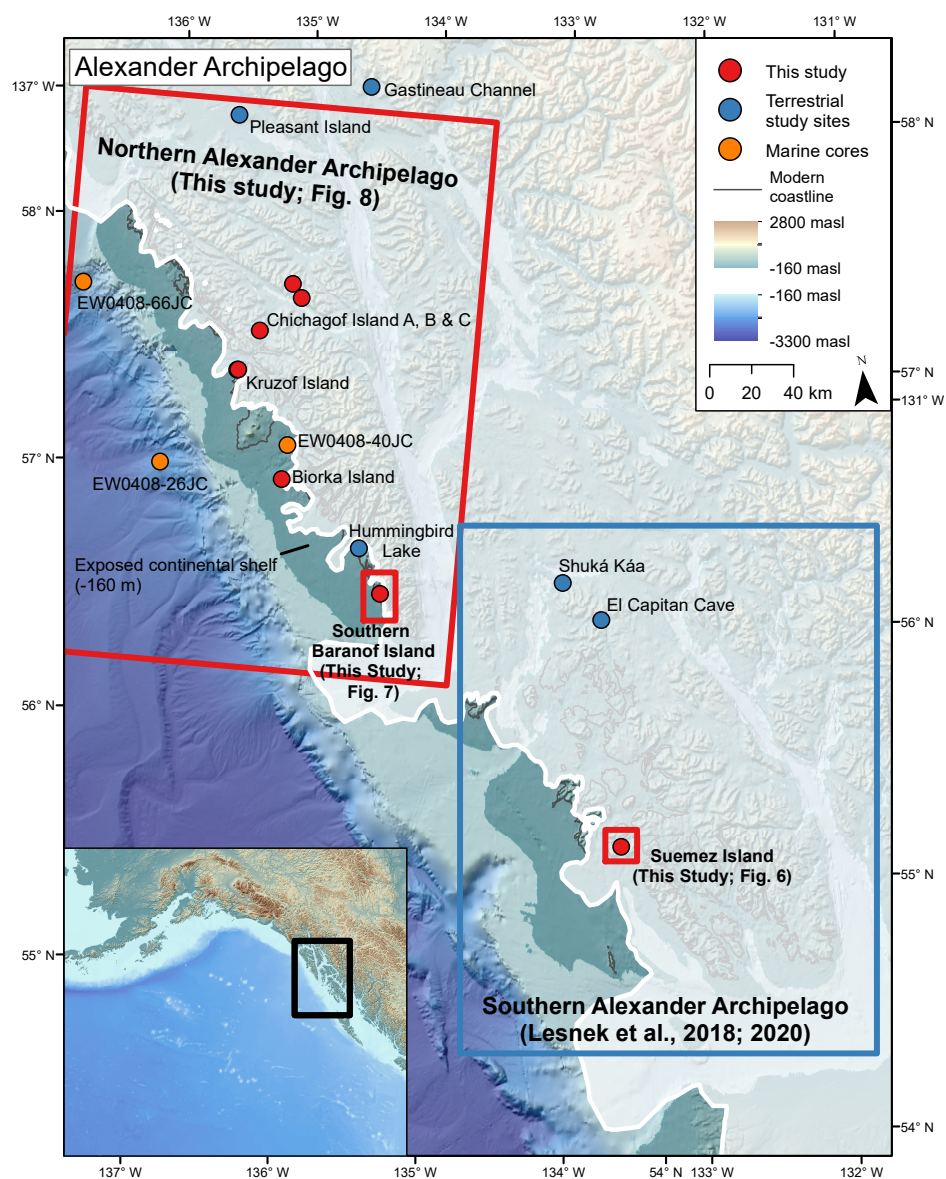
Figure 2: The Alexander Archipelago showing relevant marine sediment cores and terrestrial chronologies. Shaded white areas show hypothesized LLGM Cordilleran Ice Sheet extent (Lesnek et al., 2020). - 160 m relative sea level lowering after Baichtal et al. (2021). Red boxes and points show sampling locations from this study. Blue box shows extent of study area from Lesnek et al. (2018; 2020). Orange dots represent locations of marine sediment cores: EW0408-66JC and EW0408-26J (Praetorius and Mix, 2014; Praetorius et al., 2016) and EW0408-40JC (Addison et al., 2010). Blue dots indicate locations of relevant terrestrial study sites: Gastineau Channel (Miller, 1973), Pleasant Island (Hansen and Engstrom, 1996), Hummingbird Lake (Ager, 2019), Shuká Káa (Lesnek et al., 2018), and El Capitan Cave (Wilcox et al., 2019).

847
848
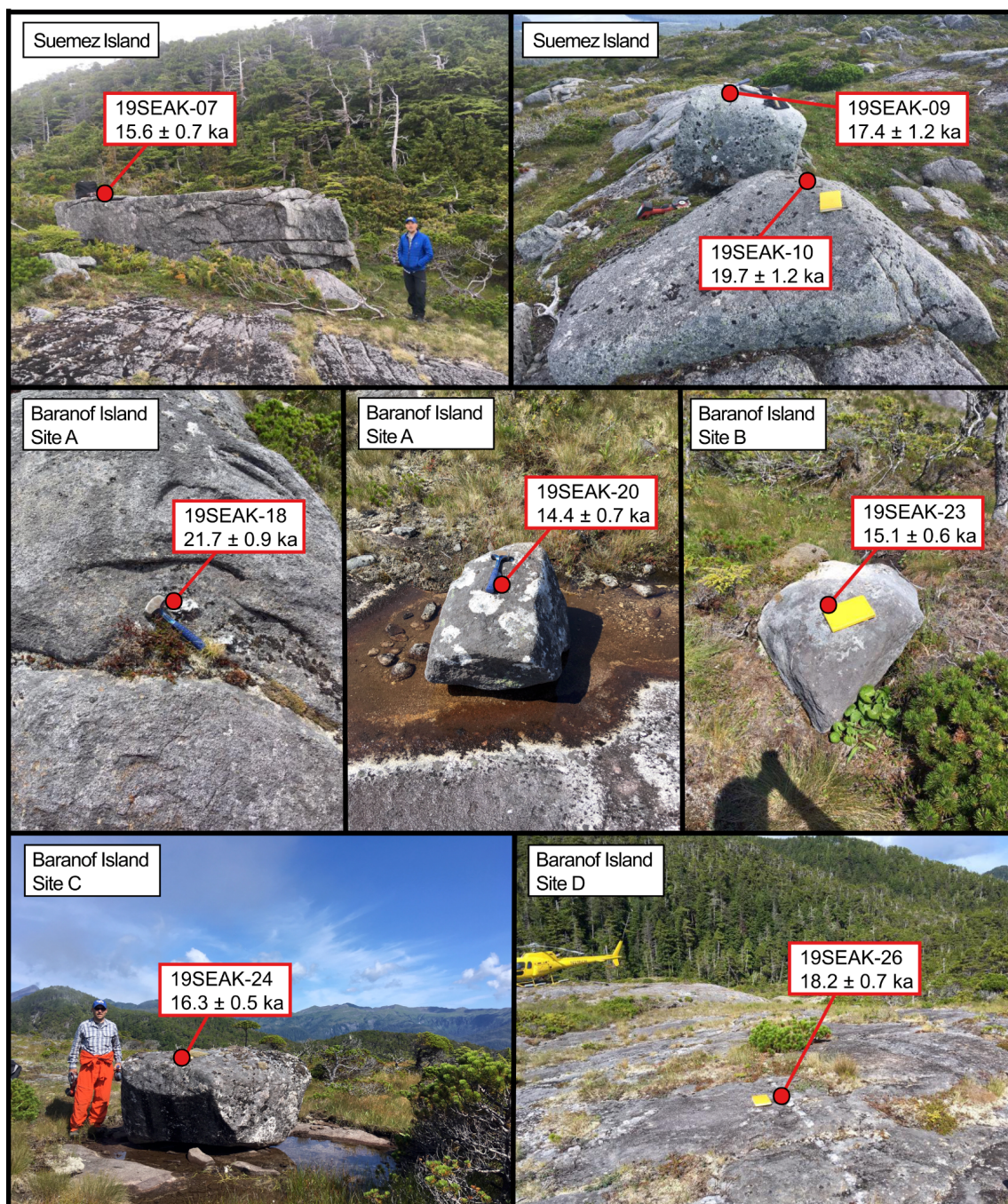
Figure 3: Sample photos from 2019 field season. All [10]Be ages shown with 1 σ internal uncertainty.

851

852

853

854

855

856

Figure 4: Sample photos from 2018 and 2020 field season. All [10]Be ages are shown with 1 σ
internal uncertainty. Note the relatively small size of 20SEAK-15.

859

860
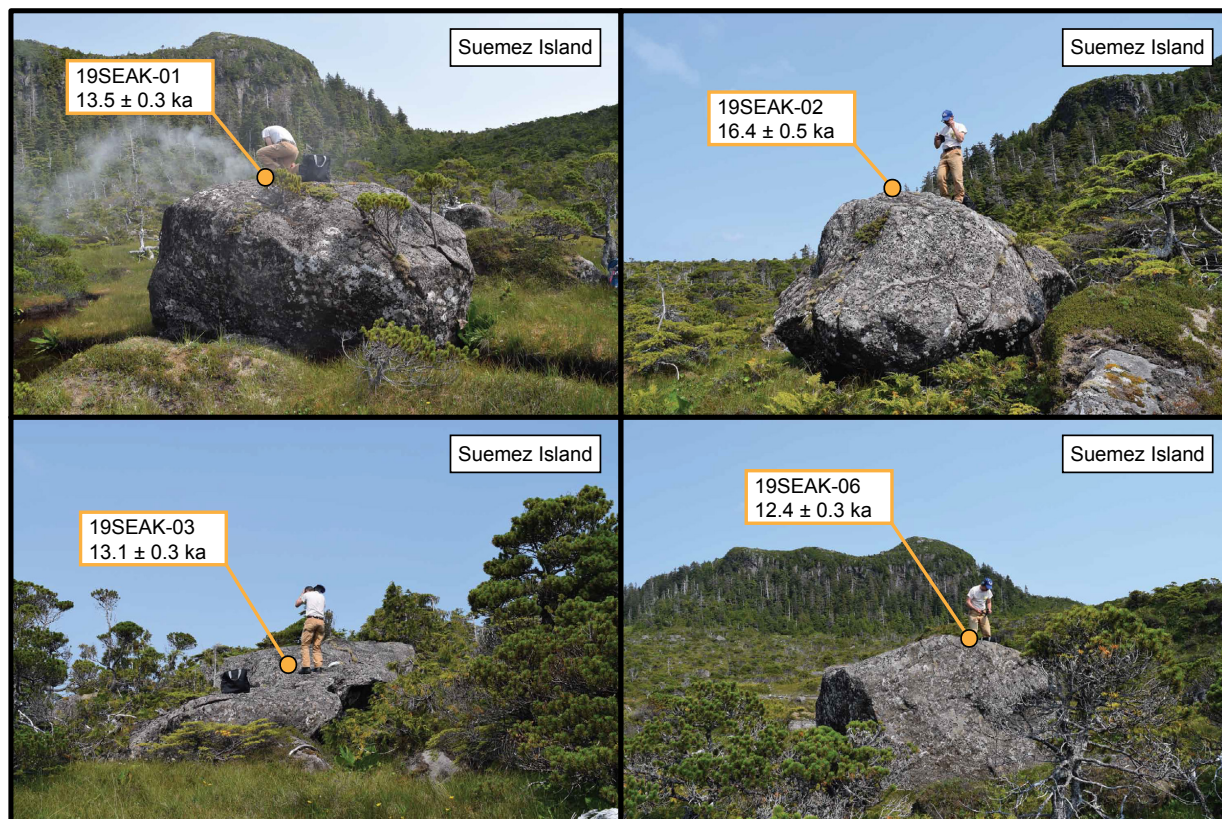
Figure 5: Basalt samples and ^{36}Cl ages from southwestern Suemez Island. Ages are reported at 1 σ internal uncertainty.

Table 1: [10]Be surface exposure age data

Sample ID	Sample type	Latitude (°N)[a]	Longitude (°W)[a]	Elevation (m asl)[a]	Boulder height (m)	Sample thickness (cm)	Topographic shielding correction	Quartz (g)	[9]Be added (µg)	[10]Be/[9]Be ratio[b]	[10]Be/[9]Be ratio uncertainty	[10]Be (atoms/g)	[10]Be uncertainty (atoms/g)	[10]Be age (ka)[c] Arctic PR	[10]Be age (ka)[c] Global PR
BIORKA ISLAND															
18JB005	Boulder	56.8482	-135.5314	47	1.0	3.0	1.0000	34.37	232	1.36E-13	4.38E-15	6.60E+04	2.12E+03	15.3 ± 0.5 (0.8)	14.7 ± 0.5 (1.2)
18JB006	Boulder	56.8471	-135.5315	43	1.2	3.0	1.0000	34.57	221	1.32E-13	4.87E-15	6.40E+04	2.35E+03	14.9 ± 0.6 (0.8)	14.3 ± 0.5 (1.2)
18JB007	Boulder	56.8527	-135.5363	46	1.0	3.0	1.0000	33.92	233	1.35E-13	4.54E-15	6.60E+04	2.23E+03	15.4 ± 0.5 (0.8)	14.8 ± 0.5 (1.1)
18JB008	Boulder	56.8528	-135.5362	46	1.0	3.0	1.0000	24.35	232	8.60E-14	2.92E-15	5.90E+04	1.99E+03	13.7 ± 0.5 (0.7)	13.2 ± 0.4 (1.1)
SUEMEZ ISLAND															
19SEAK-07	Boulder	55.2469	-133.3414	376	2.0	2.0	0.9958	21.24	233	1.25E-13	5.41E-15	9.19E+04	3.97E+03	15.6 ± 0.7 (0.9)	14.9 ± 0.6 (1.3)
19SEAK-08	Boulder	55.2470	-133.3419	392	1.0	2.0	0.9984	12.04	226	7.20E-14	5.42E-15	9.03E+04	6.80E+03	15.0 ± 1.1 (1.3)	14.4 ± 1.1 (1.5)
19SEAK-09	Boulder	55.2477	-133.3406	394	0.7	2.0	1.0000	19.44	233	1.31E-13	9.28E-15	1.05E+05	7.44E+03	17.4 ± 1.2 (1.4)	16.7 ± 1.2 (1.7)
19SEAK-10	Bedrock	55.2477	-133.3406	419	-	3.0	1.0000	17.81	213	1.38E-13	8.63E-15	1.21E+05	7.55E+03	19.7 ± 1.2 (1.4)	18.9 ± 1.2 (1.9)
BARANOF ISLAND															
Site A															
19SEAK-17	Boulder	55.3677	-134.9015	140	0.5	2.0	0.9923	25.08	233	1.30E-13	6.21E-15	8.02E+04	3.84E+03	16.9 ± 0.8 (1.0)	16.3 ± 0.8 (1.5)
19SEAK-18	Bedrock	56.3723	-134.9084	129	-	2.0	1.0000	25.24	232	1.66E-13	6.95E-15	1.02E+05	4.27E+03	21.7 ± 0.9 (1.2)	20.8 ± 0.9 (1.8)
19SEAK-19	Bedrock	56.3718	-134.9094	126	-	2.0	1.0000	24.80	233	2.10E-13	8.06E-15	1.31E+05	5.05E+03	28.0 ± 1.1 (1.5)	26.9 ± 1 (2.3)
19SEAK-20	Boulder	56.3712	-134.9082	135	0.6	2.0	1.0000	25.03	233	1.09E-13	5.59E-15	6.80E+04	3.47E+03	14.4 ± 0.7 (0.9)	13.8 ± 0.7 (1.3)
Site B															
19SEAK-21	Boulder	56.3636	-134.9068	48	0.5	2.0	1.0000	25.05	233	1.00E-13	4.57E-15	6.23E+04	2.84E+03	14.4 ± 0.7 (0.9)	13.8 ± 0.6 (1.2)
19SEAK-22	Bedrock	56.3636	-134.9072	58	-	2.0	0.9749	20.17	230	8.03E-14	3.10E-15	6.13E+04	2.36E+03	14.4 ± 0.6 (0.8)	13.8 ± 0.5 (1.2)
19SEAK-23	Boulder	56.3638	-134.9092	68	0.5	2.0	0.9911	20.24	231	8.64E-14	3.29E-15	6.60E+04	2.51E+03	15.1 ± 0.6 (0.8)	14.5 ± 0.6 (1.2)
Site C															
19SEAK-24	Boulder	56.3228	-134.892	150	1.0	1.5	1.0000	20.12	234	1.01E-13	3.39E-15	7.83E+04	2.63E+03	16.3 ± 0.5 (0.8)	15.6 ± 0.5 (1.3)
19SEAK-25	Bedrock	56.3231	-134.8916	163	-	1.5	1.0000	19.99	234	9.80E-14	3.41E-15	7.68E+04	2.67E+03	15.7 ± 0.6 (0.8)	15.1 ± 0.5 (1.3)
Site D															
19SEAK-26	Bedrock	56.3554	-134.8856	145	-	2	0.9879	25.12	235	1.37E-13	5.54E-15	8.56+04	3.47E+03	18.2 ± 0.7 (1.0)	17.4 ± 0.7 (1.5)
19SEAK-27	Bedrock	56.3555	-134.8855	142	-	1.5	0.9963	25.04	233	1.54E-13	5.89E-15	9.59E+04	3.67E+03	20.2 ± 0.8 (1.1)	19.3 ± 0.7 (1.6)
KRUZOF ISLAND															
20SEAK-7	Boulder	57.3112	-135.8126	558	2.5	1.5	0.9976	20.14	233	1.36E-13	7.24E-15	1.05E+05	5.59E+03	14.9 ± 0.8 (1.0)	14.3 ± 0.8 (1.3)
20SEAK-10	Bedrock	57.3112	-135.8111	559	-	1.5	0.96912	20.13	231	1.20E-13	8.48E-15	9.23E+04	6.50E+03	13.4 ± 1.0 (1.1)	12.9 ± 0.9 (1.3)
20SEAK-12	Boulder	57.3110	-135.8110	569	1.0	1.0	0.9927	20.07	382	8.32E-14	3.74E-15	1.06E+05	4.77E+03	14.9 ± 0.7 (0.9)	14.3 ± 0.6 (1.3)
20SEAK-13	Boulder	57.3109	-135.8109	568.3	1.5	1.0	0.9941	20.25	230	1.36E-13	7.43E-15	1.04E+05	5.65E+03	14.6 ± 0.8 (1.0)	14.1 ± 0.8 (1.3)
CHICHAGOF ISLAND															
Site A															
20SEAK-14	Bedrock	57.4621	-135.6354	476	-	0.5	1.0000	20.25	230	1.34E-13	6.34E-15	1.01E+05	4.80E+03	15.3 ± 0.7 (0.9)	14.6 ± 0.7 (1.3)
20SEAK-15	Boulder	57.4621	-135.6354	476	0.3	1.0	1.0000	20.33	227	1.13E-13	6.04E-15	8.38E+04	4.50E+03	12.7 ± 0.7 (0.8)	12.2 ± 0.7 (1.1)
20SEAK-16	Boulder	57.4618	-135.6351	473	0.3	1.5	1.0000	20.26	240	7.48E-14	4.78E-15	5.92E+04	3.78E+03	9.0 ± 0.6 (0.7)	8.6 ± 0.6 (0.9)
Site B															
20SEAK-18	Boulder	57.5743	-135.2721	817	0.5	3.0	1.0000	15.20	226	1.09E-13	7.99E-15	1.09E+05	7.99E+03	12.4 ± 0.9 (1.0)	11.8 ± 0.9 (1.2)
20SEAK-19	Bedrock	57.5743	-135.2720	816	-	1.5	1.0000	20.05	239	1.57E-13	7.31E-15	1.25E+05	5.81E+03	14.1 ± 0.7 (0.8)	13.5 ± 0.6 (1.2)
Site C															
20SEAK-22	Bedrock	57.6425	-135.3483	779	-	2.0	1.0000	20.12	231	1.98E-13	8.58E-15	1.52E+05	6.59E+03	17.7 ± 0.8 (1.0)	17.0 ± 0.7 (1.5)

[a] Elevations and positions were recorded with a Garmin handheld GPS receiver (~5 m vertical uncertainty) or GAIA GPS (~5 m vertical uncertainty).

[b] AMS results from PRIME Lab are standardized to 07KNSTD (Nishiizumi et al., 2007); ratios are blank corrected and shown at 1 SD uncertainty.

[c] [10]Be ages reported with one σ internal uncertainties; external uncertainties in parentheses; calculated with CRONUS-Earth calculator v. 3 (Balco et al., 2008) using the Arctic production rate (Young et al., 2013) or global production rate (Borchers et al., 2016) and Lm scaling.

Table 2: ^{36}Cl surface exposure age data

Sample ID	Sample type	Latitude (°N)[a]	Longitude (°W)[a]	Elevation (m asl)[a]	Boulder height (m)	Sample thickness (cm)	Density (g/cm³)	Topographic Shielding Correction	Aliquot dissolved for total Cl determination (g)	^{37}Cl-enriched Cl added to total Cl aliquot (µg)[b]	^{35}Cl/^{37}Cl[b]	Total Cl concentration (µg/g)	Rock sample dissolved (g)	Natural Cl carrier added (µg)[c]	^{36}Cl/Cl	^{36}Cl/Cl Uncertainty[d]	^{36}Cl concentration (atoms/g)[e]	^{36}Cl concentration uncertainty (atoms/g)[e]	^{36}Cl age (ka)[f]
ROCK SAMPLES																			
19SEAK-01[g]	Boulder	55.2449	-133.4328	391	2.0	2.5	2.8	0.995658	1.2063	75.4	1.110	12.9 ± 0.8	12.0014	358	1.47E-13	3.39E-15	1.03E+05	2.41E+03	13.5 ± 0.3 (1.3)
19SEAK-02[h]	Boulder	55.2461	-133.4327	398	2.5	3	2.8	0.994066	1.0383	76.2	1.014	5.7 ± 0.1	11.5081	435	1.74E-13	5.07E-15	1.27E+05	3.73E+03	16.4 ± 0.5 (1.5)
19SEAK-03[i]	Boulder	55.246	-133.4324	398	2.0	2.5	2.8	0.994066	1.2061	76.5	1.282	24.0 ± 0.8	14.0301	171	2.00E-13	4.34E-15	1.22E+05	2.67E+03	13.1 ± 0.3 (1.3)
19SEAK-06[i]	Boulder	55.2448	-133.4355	398	3.0	2	2.8	0.995524	1.2081	79.5	1.088	9.3 ± 0.6	20.0269	314	2.43E-13	5.09E-15	1.03E+05	2.16E+03	12.4 ± 0.3 (1.1)
PROCESS BLANKS																			
CLBLK-AQ4	-	-	-	-		-	-	-	-	78.0	0.953		-	-	-	-	-		-
CLBLK-AQ6	-	-	-	-		-	-	-	-	78.0	0.938		-	-	-	-	-		-
CLBLK-AQ8	-	-	-	-		-	-	-	-	76.6	0.936		-	-	-	-	-		-
CLBLK-26	-	-	-	-		-	-	-	-	-	-		-	0.1998	2.37E-15	9.24E-16	-		-

[a] Elevations and positions were recorded with a Garmin handheld GPS receiver (~5 m vertical uncertainty) or GAIA GPS (~5 m vertical uncertainty).

[b] The 37Cl-enriched spike was made at Lawrence Livermore National Laboratory. Its Cl concentration is 1285 ppm and its 35Cl/37Cl ratio is 0.93.

[c] The natural Cl carrier was made by dissolving Weeks Island Halite in deionized water at the University of New Hampshire. Its Cl concentration is 1436 ± 9 ppm and its ^{35}Cl/^{37}Cl ratio is 3.127.

[d] Uncertainties on ^{35}Cl/^{37}Cl and ^{36}Cl/Cl ratios and exposure ages represent propagated 1σ analytical uncertainties only

[e] Sample 36Cl concentrations are corrected for 36Cl contributed by process blank CLBLK-26

[f] Exposure ages are presented at 1 σ internal uncertainty; external uncertainty shown in parentheses. Ages were calculated with the CRONUSEarth 36Cl calculator (http://stoneage.ice-d.org/math/Cl36/v3/v3_Cl36_age_in.html) and Lm scaling (Lal, 1991) assuming no surface erosion and steady state nucleogenic ^{36}Cl production.

[g] Aliquot for stable Cl measurements processed with CLBLK-AQ6

[h] Aliquot for stable Cl measurements processed with CLBLK-AQ8

[i] Aliquot for stable Cl measurements processed with CLBLK-AQ4
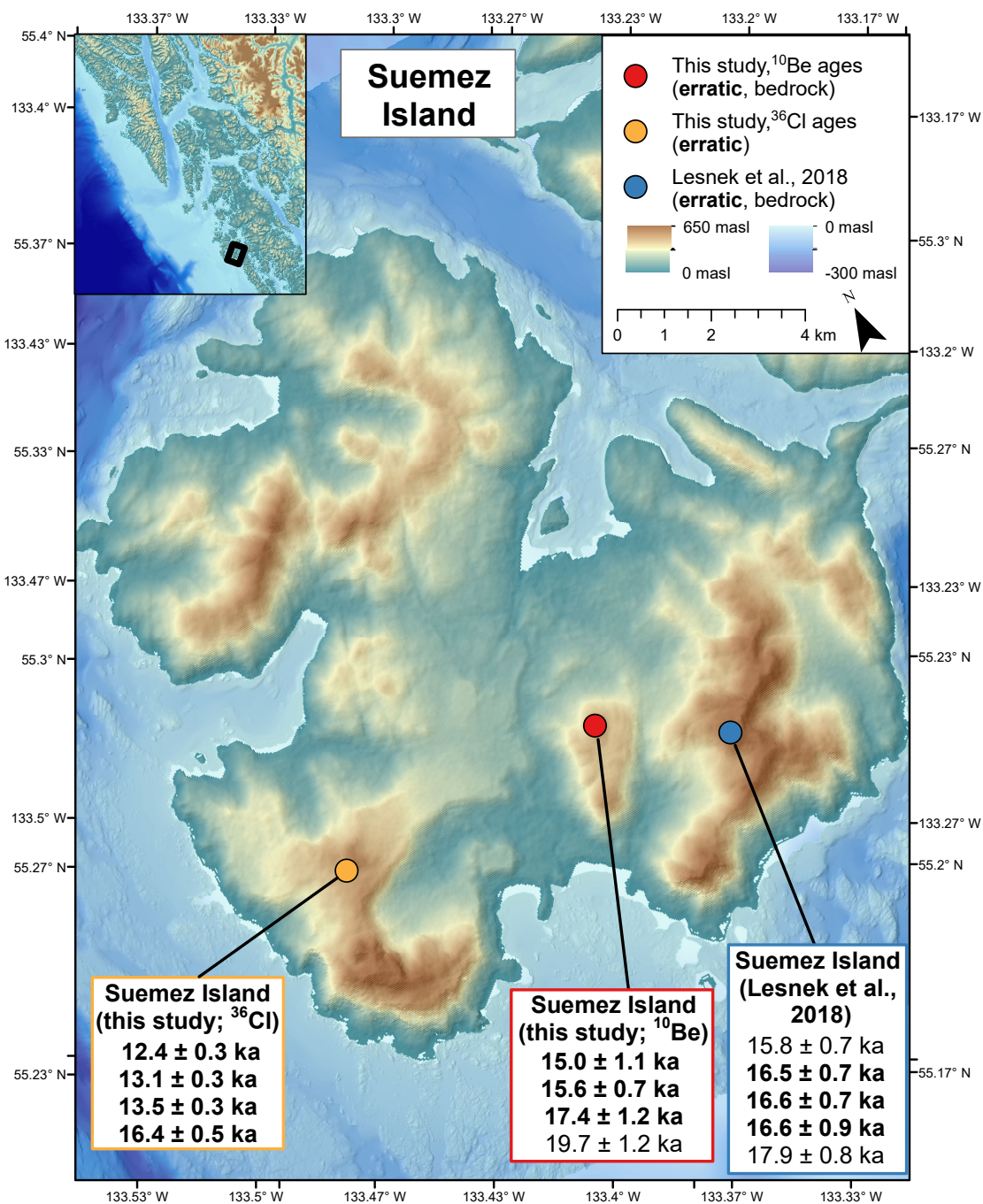
Figure 6: [10]Be and [36]Cl ages from samples collected on Suemez on island: red and yellow dots mark sampling site from this study, blue dot marks sampling site from Lesnek et al.(2018). Bold ages are from boulders; plain ages are from bedrock. All [10]Be and [36]Cl ages reported with 1 σ internal uncertainty.
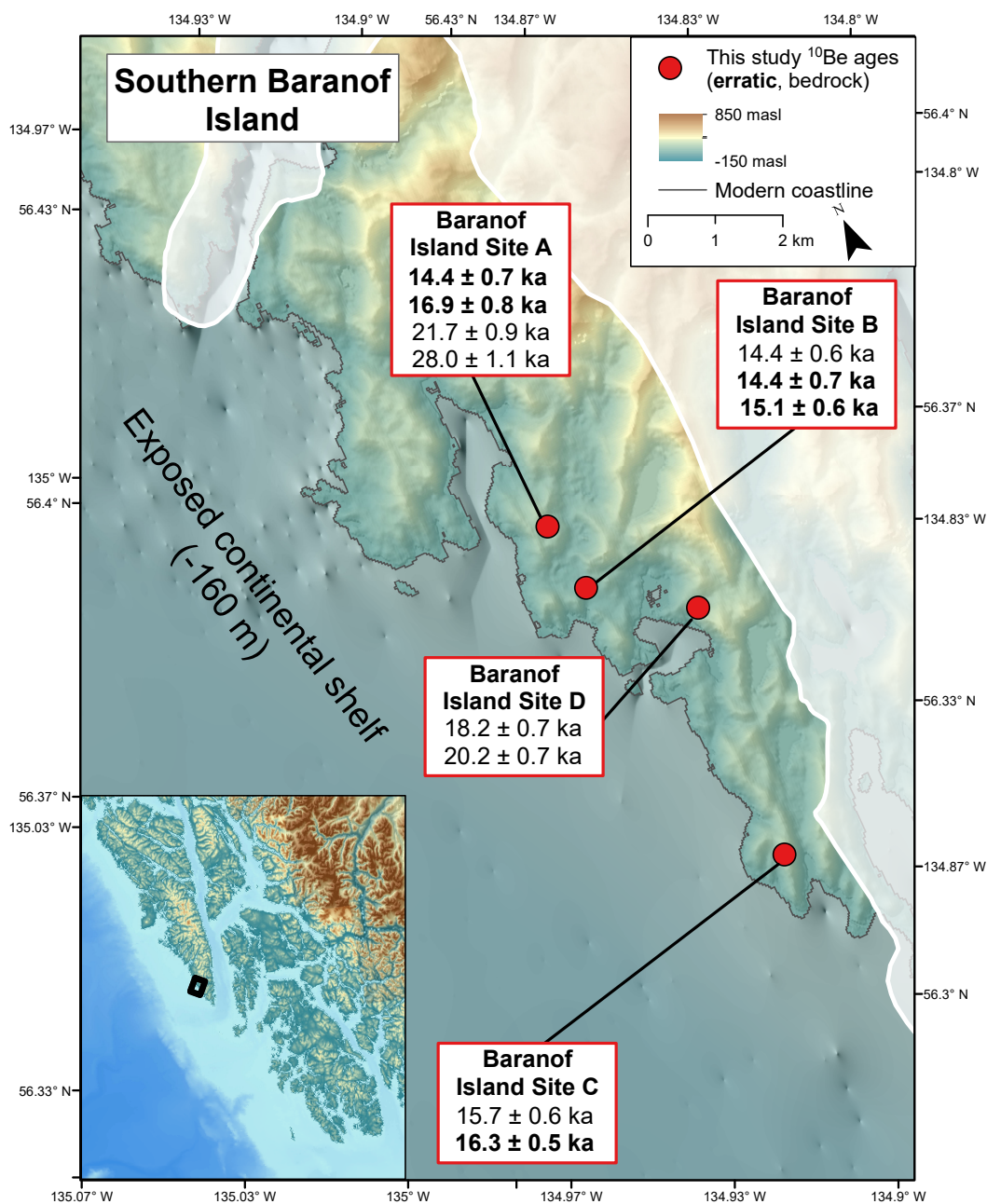
Figure 7: [10]Be ages from sampling sites on southern Baranof Island. Bold ages are from boulders; plain ages are from bedrock. All ages are reported with 1 σ internal error. Cordilleran Ice Sheet LLGM extent after Carrara et al. (2007).
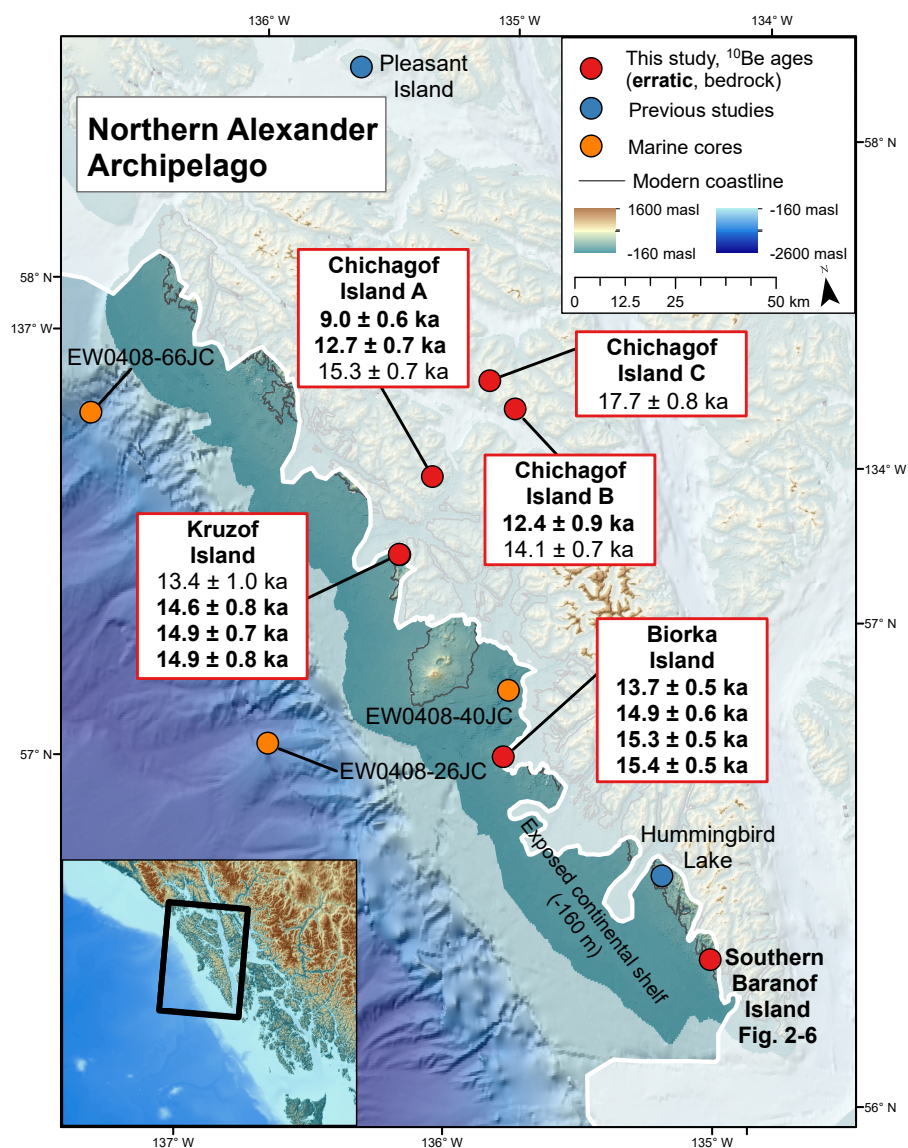
Figure 8: ^{10}Be ages from sampling sites in the northern Alexander Archipleago. All ages are reported with 1 σ internal error. Bold ages are from boulders; plain ages are from bedrock.. LLGM Cordilleran Ice Sheet extent after Lesnek et al. (2020). Exposed continental shelf at -160 m below modern sea level Baichtal et al. (in press). Yellow dots show location of relevant marine sediment cores: EW0408-66JC and EW0408-26JC (Praetorius and Mix, 2014; Praetorius et al., 2016) and EW0408-40JC (Addison et al., 2010). Blue dots show locations of relevant terrestrial study sites: Pleasant Island (Hansen and Engstrom, 1996) and Hummingbird Lake (Ager, 2019).
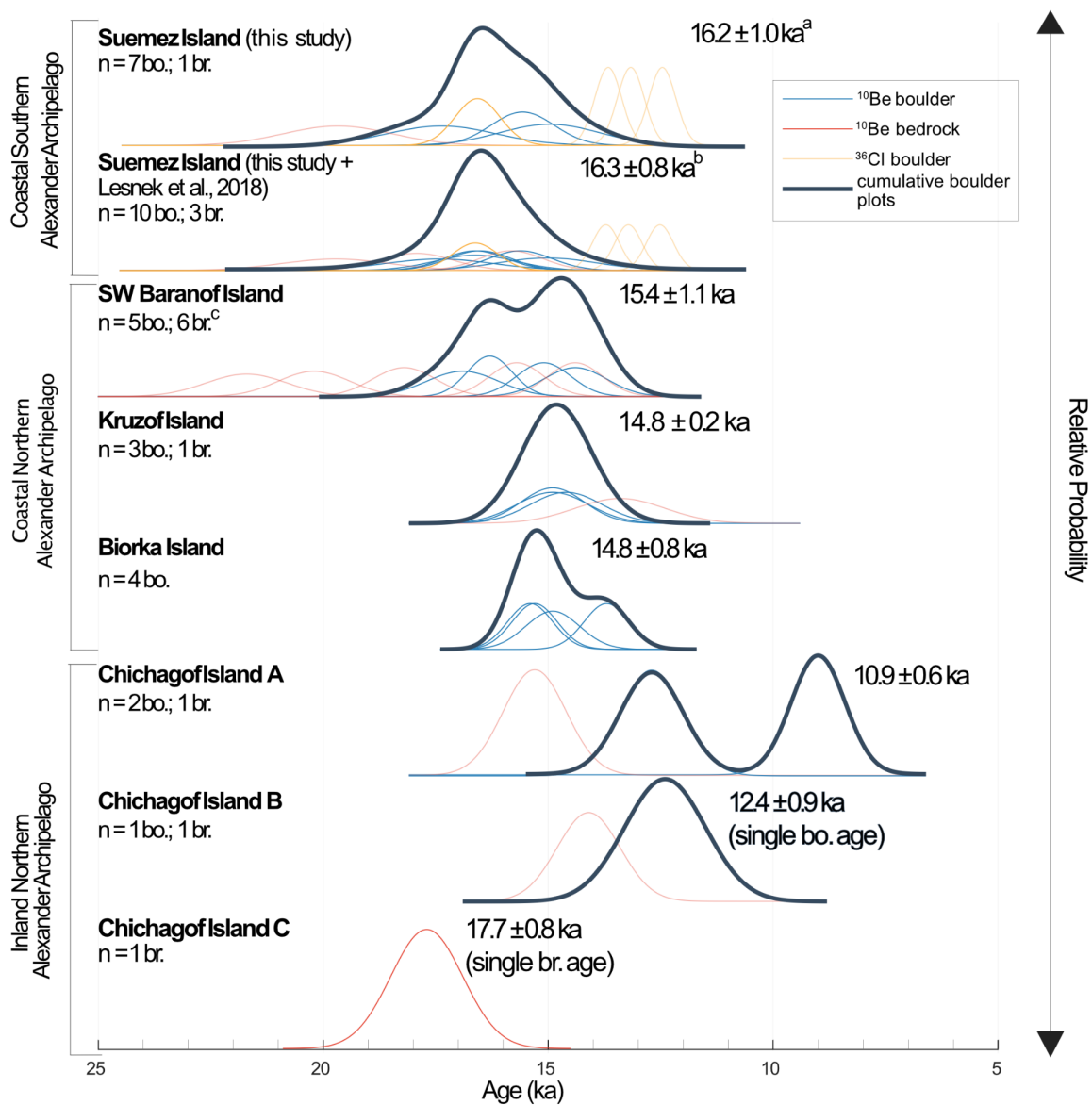
Figure 9: Relative probably plots of bedrock (red) and boulder (blue) [10]Be and [36]Cl boulder (yellow) ages from this study calculated with 1 σ internal uncertainty. bo. = boulder, br. = bedrock. All ages shown are mean ages from only boulders at each sample site reported with 1 SD unless noted. Cumulative plots represent all bold lines - transparent lines were not included in their calculation. [a]Average of all [10]Be boulder ages and oldest [36]Cl boulder age with 1 SD. [b]Average of all [10]Be boulder ages (this study and Lesnek et al., 2018) and oldest [36]Cl boulder age (this study). [c]One old outlier at 28.0 ± 1.1 ka not shown.
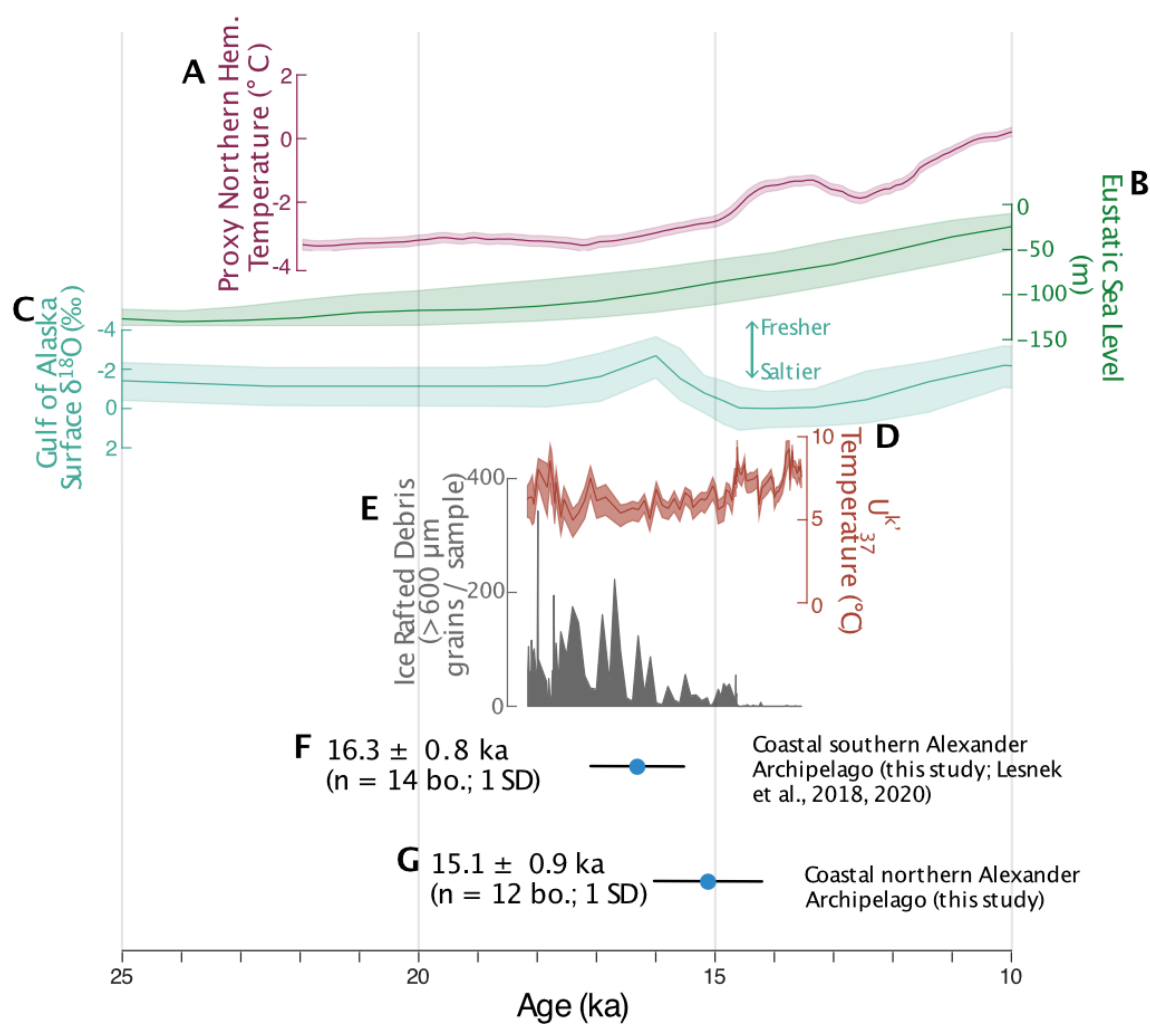
Figure 10: A) Proxy Northern Hemisphere temperature anomaly relative to early Holocene with 1 σ error (Shakun et al., 2012). B) Eustatic sea-level curve (Spratt and Lisiecki, 2016). C) Gulf of Alaska surface salinity δ18O record (Core SO202-27-6; Maier et al., 2018). D) UK'37 temperature reconstruction from off the coast of the Alexander Archipelago (Cores EW0408-26JC, EW0408- 66JC; Praetorius et al., 2016). E) Ice rafted debris record from off Vancouver Island (Core MD02-2496; Cosma et al., 2008). F) & G) Meanboulder ¹⁰Be ages from the coastal Alexander Archipelago, with 1 σ r (this study; Lesnek et al., 2018; 2020).